

Platelet Membrane-Camouflaged Magnetic Nanoparticles for Ferroptosis-Enhanced Cancer Immunotherapy

Qin Jiang, Kuang Wang, Xingyu Zhang, Boshu Ouyang, Haixia Liu, Zhiqing Pang,* and Wuli Yang*

Although cancer immunotherapy has emerged as a tremendously promising cancer therapy method, it remains effective only for several cancers. Photoimmunotherapy (e.g., photodynamic/photothermal therapy) could synergistically enhance the immune response of immunotherapy. However, excessively generated immunogenicity will cause serious inflammatory response syndrome. Herein, biomimetic magnetic nanoparticles, Fe₃O₄-SAS @ PLT, are reported as a novel approach to sensitize effective ferroptosis and generate mild immunogenicity, enhancing the response rate of non-inflamed tumors for cancer immunotherapy. Fe₃O₄-SAS@PLT are built from sulfasalazine (SAS)-loaded mesoporous magnetic nanoparticles (Fe₃O₄) and platelet (PLT) membrane camouflage and triggered a ferroptotic cell death via inhibiting the glutamate-cystine antiporter system X_c⁻ pathway. Fe₃O₄-SAS @ PLT-mediated ferroptosis significantly improves the efficacy of programmed cell death 1 immune checkpoint blockade therapy and achieves a continuous tumor elimination in a mouse model of 4T1 metastatic tumors. Proteomics studies reveal that Fe₃O₄-SAS @ PLT-mediated ferroptosis could not only induce tumor-specific immune response but also efficiently repolarize macrophages from immunosuppressive M2 phenotype to antitumor M1 phenotype. Therefore, the concomitant of Fe₃O₄-SAS @ PLT-mediated ferroptosis with immunotherapy are expected to provide great potential in the clinical treatment of tumor metastasis.

1. Introduction

Cancer immunotherapy has been considered a tremendously promising cancer treatment, which stimulates inherent immune responses to combat tumor cells.^[1] By blocking negative immune regulatory pathways with antibodies to reactivate the immune system of body,^[2] immune checkpoint blockade therapy has achieved several clinical successes in recent years.^[3] However, due to the complexity of the tumor microenvironment and the inactivation of host immune systems, most of those immunotherapeutic strategies still have limitations in eliciting systemic antitumor responses for many cancers.^[4a,b] Moreover, tumor cells can protect themselves from immune attack through immune escape and immunosuppression.^[4c,4d] Reversing tumor immunosuppression and enhancing anti-tumor immunity are the most challenges of immunotherapy. Synergistic combination of checkpoint blockade therapy with other immunogenic therapeutics may be a feasible approach to increase the immune response rates of non-inflamed tumors.^[5] For instance,

photothermal/photodynamic therapy using nanoparticles, can effectively generate a vaccine-like immune response,^[6,7] and has been shown to induce antigen-specific immunological responses from tumor residues, thereby enhancing immunotherapy efficacy. However, it has been reported that over-generated immunogenicity could not induce an effective immune response,^[8] but cause the systemic inflammatory response syndrome and serious complications associated with multiple organ dysfunction syndrome.^[9] Moreover, most nanoparticle-based photodynamic/photothermal therapies still have limitations, such as limited light penetration, oxygen dependence, as well as limited therapeutic efficacies,^[10,11] resulting in less-than-perfect clinical outcomes. Therefore, developing new approaches and strategies to effectively induce immune response and enhance antitumor response is of great significance for cancer immunotherapy.

Ferroptosis is a new cell death format identified in recent years.^[12] It can be activated by the inactivation of glutathione peroxidase 4 (GPX4), thereby breaking balance between the producing and scavenging of intracellular reactive oxygen species (ROS, mainly hydroxyl radicals).^[13] The excessive production and

Dr. Q. Jiang, K. Wang, H. Liu, Prof. W. Yang
 State Key Laboratory of Molecular Engineering of Polymers
 Department of Macromolecular Science
 Fudan University
 Shanghai 200433, P. R. China
 E-mail: wlyang@fudan.edu.cn

X. Zhang
 Department of Sports Medicine
 Huashan Hospital
 Fudan University
 Shanghai 200040, P. R. China

B. Ouyang, Prof. Z. Pang
 Key Laboratory of Smart Drug Delivery
 Ministry of Education
 Department of Pharmaceutics
 School of Pharmacy
 Fudan University
 Shanghai 201203, P. R. China
 E-mail: zqpang@fudan.edu.cn

 The ORCID identification number(s) for the author(s) of this article can be found under <https://doi.org/10.1002/smll.202001704>.

DOI: 10.1002/smll.202001704

accumulation of oxidative hydroxyl radicals further leads to elevation of lipid peroxidation to initiate ferroptosis.^[14] Ferroptosis can effectively inhibit tumor growth and generate mild immunogenicity, which is totally different from apoptosis, necroptosis, and autophagy.^[15] Considering the central role of iron in ferroptosis, many studies have focused on iron-based nanomaterials such as ferumoxytol,^[16] inorganic iron nanoparticles,^[17] and iron-organic frameworks^[18] for cancer treatment. These nanomaterials have displayed potential to improve the effectiveness of ferroptosis in cancer treatment, but few have clinical applications because of lack of immune evasion and poor tumor targeting.^[19]

Recently, due to their self-recognition properties, cell membranes derived from such as red blood cells, platelets, and macrophages have been used to camouflage nanoparticles to evade the immune clearance.^[20] These cell membrane-camouflaged nanoparticles have been demonstrated to be effective for immune modulation.^[20c] Specifically, platelet membrane-camouflaged nanoparticles have been widely used in targeted therapy of cancers because of the innate advantages of platelets, such as quickly responding to vascular damage, and recognizing and interacting with circulating tumor cells.^[21] In addition, biomimetic nanoparticles derived from platelet membranes have been demonstrated to prolong blood circulation and reduce hepatic uptake.^[22] Hence, platelet membrane-camouflaged nanoparticles with immune evasion and tumor targeting abilities can maximize the delivery of ferroptosis-inducing nanoparticles to tumors, thus showing full potential in ferroptosis therapy of tumor metastasis.

Herein, we report a ferroptosis-enhanced cancer immunotherapy strategy that combines ferroptosis induced by biomimetic nanoparticles and the programmed cell death 1 (PD-1) immune checkpoint blockade therapy (**Scheme 1**). Sulfasalazine (SAS), as a very important drug for the treatment of rheumatoid, not only inhibits the migration of inflammatory cells and I κ B kinase pathway,^[23] but also restrains the uptake of cysteine to suppress tumor growth and induce ferroptosis.^[24a] The activity of SAS has been demonstrated in preclinical cancer models,^[24b,c] however, it must be used at high concentration.^[24d] Therefore, we loaded SAS into magnetic nanoparticles (Fe₃O₄) and camouflaged by platelet membranes (Fe₃O₄-SAS@PLT) for tumor ferroptosis treatment. Fe₃O₄ nanoparticles are also ferroptosis inducer, which can work synergistically together with SAS spatially and temporally, greatly reducing the dosage of SAS. The platelet membrane coating endowed Fe₃O₄-SAS@PLT with the abilities of immune evasion and targeting to tumor metastasis. After intravenous injection, Fe₃O₄-SAS@PLT can accumulate at the tumor sites. Fe₃O₄-SAS@PLT-mediated ferroptosis can elicit an effective immune response, which significantly promote PD-1 blockade therapy in a mouse model of metastatic 4T1 tumors. In addition, proteomic analysis was performed to elucidate the mechanisms by which Fe₃O₄-SAS@PLT-mediated ferroptosis enhanced the anti-tumor immune response.

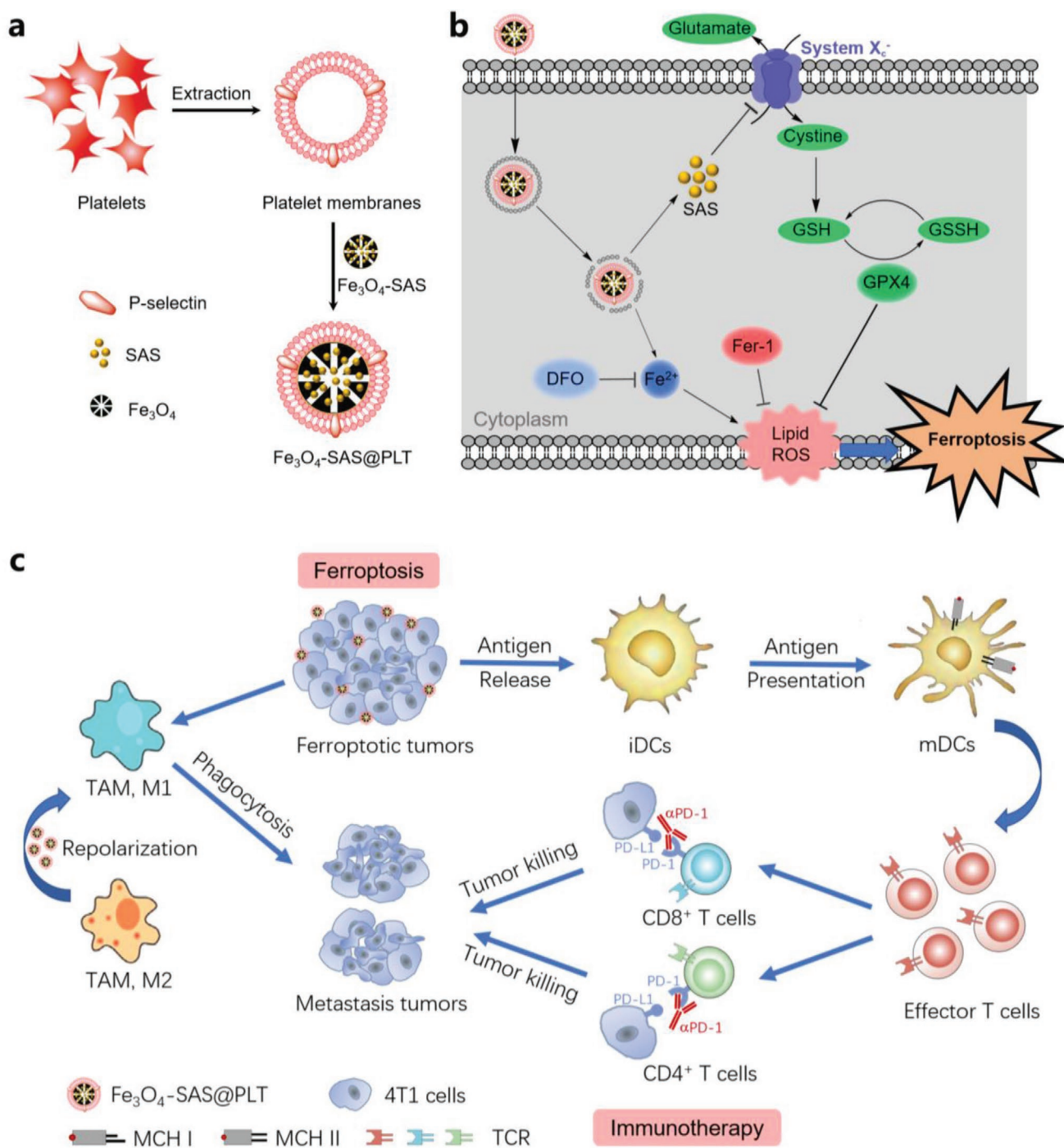
2. Results and Discussion

2.1. Formulation and Characterization of Fe₃O₄-SAS@PLT

Platelets (PLTs) were circulating guards in the blood stream that have chemotaxis effect to the damaged vasculatures and tumor

tissues.^[25] Recent studies have demonstrated that PLT membranes can be used as a biomimetic coating to endow nanoparticles with the abilities of avoiding macrophage recognition, capturing circulating tumor cells, and homing to the inflammatory sites,^[26,27a] and so on. The PLT membrane-camouflaged Fe₃O₄-SAS (magnetic nanoparticle loaded with sulfasalazine (SAS)) nanoparticles (designated as Fe₃O₄-SAS@PLT) were prepared via an extrusion method reported previously (Scheme 1a).^[21] Compared with bare Fe₃O₄-SAS, the prepared Fe₃O₄-SAS@PLT had a clear core/shell structure (**Figure 1a**), indicating the presence of a unilamellar cell membrane coating on the nanoparticle. The thickness of the outer shell was \approx 10 nm, indicating that the PLT membrane provided prominent coverage to the nanoparticles. The average hydrodynamic diameter of Fe₃O₄-SAS@PLT was 268.9 ± 8.9 nm (**Figure 1b**), which was slightly greater than that of bare Fe₃O₄-SAS (242.3 ± 2.0 nm). The average zeta potential of Fe₃O₄-SAS@PLT was -22.1 ± 0.9 mV, similar to that of PLT membrane vesicles (-23.0 ± 0.5 mV) but significantly lower than that of bare Fe₃O₄-SAS (-14.1 ± 0.8 mV), reflecting the successful coating of PLT membranes on nanoparticles. Then, the colloidal stability of Fe₃O₄-SAS@PLT was examined by measuring the size changes over time. Fe₃O₄-SAS@PLT showed negligible size change and a low polydispersity index (PDI) for 7 days (**Figure 1c**). Even after incubation in 10% fetal bovine serum-containing phosphate buffer saline (PBS) over a week at 4 °C, the size of Fe₃O₄-SAS@PLT was still around 280 nm with a narrow PDI (**Figure 1d**) while that of bare Fe₃O₄-SAS significantly increased (684 ± 34 nm). In addition, after PLT membrane camouflage, the relative turbidity of Fe₃O₄-SAS@PLT-treated platelet-rich plasma exhibited a negligible change within 60 min in comparison with that of PBS group (**Figure S1**, Supporting Information). Collectively, these results demonstrated the excellent plasma stability of Fe₃O₄-SAS@PLT in the biological environment.

By utilizing sodium dodecyl sulfate-polyacrylamide gel electrophoresis (SDS-PAGE), we analyzed the composition of cell membrane proteins on the surface of Fe₃O₄-SAS@PLT. Fe₃O₄-SAS@PLT exhibited protein bands similar to the PLT membrane vesicles and the PLT membranes (**Figure 1e**), indicating the effective translocation of PLT membranes on the surface of Fe₃O₄-SAS@PLT. Especially, the specific protein markers were analyzed by using western blotting (**Figure 1f**). CD47 (48 kDa), an immunomodulatory protein that can prevent macrophage uptake,^[28a] was detected on the PLT membranes, PLT membrane vesicles, and Fe₃O₄-SAS@PLT. CD41 (113 kDa) and P-selectin (also known as CD62p, 91 kDa), two important glycoproteins for platelet adhesion, aggregation, and activation,^[28b] were also maintained on the PLT membranes, PLT membrane vesicles, and Fe₃O₄-SAS@PLT. Semi-quantification of band intensity on western blotting revealed no noticeable difference in the expression of CD47, CD41, as well as P-selectin between Fe₃O₄-SAS@PLT and control groups. To further elucidate the functional activity of PLT membrane proteins retained on Fe₃O₄-SAS@PLT, we measured the CD41 protein activity with flow cytometry through the binding of CD41 protein with its primary antibody (CD41-Alexa Fluor488). As shown in **Figure 1g**, Fe₃O₄-SAS@PLT, enwrapped in PLT membranes, had a much more prominent fluorescence reinforcement than bare Fe₃O₄-SAS, suggesting the success incorporation of functional properties from platelets onto Fe₃O₄-SAS@PLT.



Scheme 1. Schematic illustration of platelet membrane-camouflaged magnetic nanoparticles for ferroptosis-enhanced cancer immunotherapy. a) Preparation of Fe_3O_4 -SAS@PLT. b) Fe_3O_4 -SAS@PLT-induced cell death by ferroptosis. c) Mechanisms of Fe_3O_4 -SAS@PLT-mediated ferroptosis enhancing immune checkpoint blockade in metastasis tumors.

The drug loading capacity (DLC) and encapsulation efficiency (EE) of SAS in Fe_3O_4 -SAS@PLT were quantified by reading the absorbance of SAS at 359 nm (Figure S2, Supporting Information). The DLC and EE of SAS in Fe_3O_4 -SAS@PLT were calculated to be 20.1% and 78.5%, respectively, very close to those of Fe_3O_4 -SAS nanoparticles (DLC: 20.8%, EE: 78.6%), suggesting little loss of SAS during the PLT membrane coating.

Then, the *in vitro* release behavior of SAS from Fe_3O_4 -SAS@PLT was determined at 37 °C under different pH conditions. Fe_3O_4 -SAS@PLT exhibited a lower SAS release compared with Fe_3O_4 -SAS under physiological conditions (pH = 7.4) (Figure S3, Supporting Information), which was probably attributed to the coverage of PLT membranes on nanoparticles. The low release rate would be greatly beneficial in reducing drug leakage into

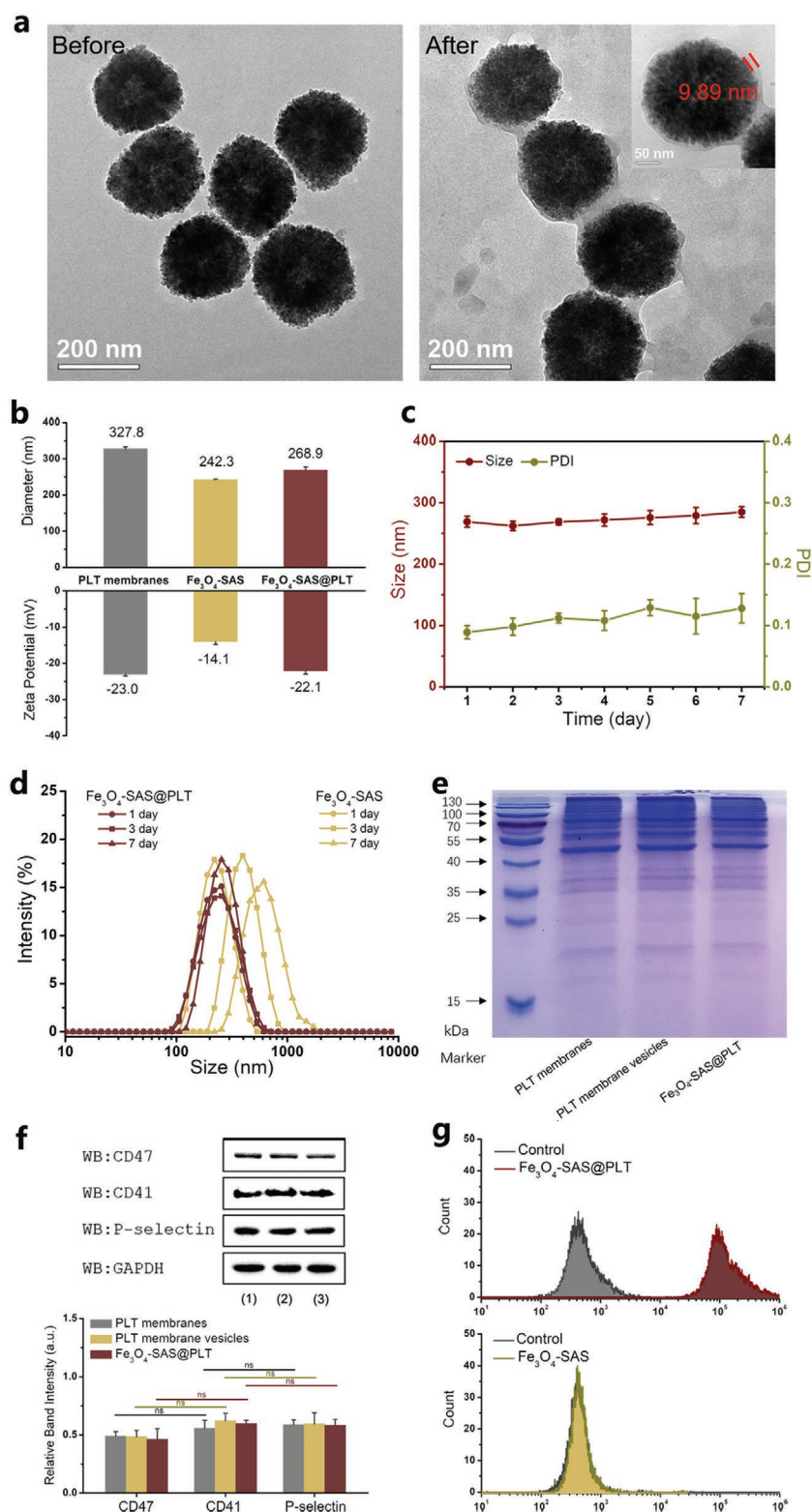


Figure 1. Formulation and characterization of $\text{Fe}_3\text{O}_4\text{-SAS@PLT}$. a) TEM images showing the morphologies of $\text{Fe}_3\text{O}_4\text{-SAS}$ before and after PLT membrane coating. Scale bar: 200 nm; scale bar in inset: 50 nm. b) Hydrodynamic diameters and zeta potentials of PLT membranes, $\text{Fe}_3\text{O}_4\text{-SAS}$, and $\text{Fe}_3\text{O}_4\text{-SAS@PLT}$; $n = 3$. c) Change in size of $\text{Fe}_3\text{O}_4\text{-SAS@PLT}$ in PBS for 7 days; $n = 3$. d) Stability of $\text{Fe}_3\text{O}_4\text{-SAS@PLT}$ in 10% fetal bovine serum-containing phosphate buffer saline over a week. e) Analysis of protein composition of PLT membranes, PLT membrane vesicles, and $\text{Fe}_3\text{O}_4\text{-SAS@PLT}$ by SDS-PAGE. f) Analysis of CD47, CD41, P-selectin proteins in PLT membranes 1), PLT membrane vesicles 2), and $\text{Fe}_3\text{O}_4\text{-SAS@PLT}$ 3) by western blotting; $n = 3$; ns represented no significance. g) Analysis of CD41 protein activity on $\text{Fe}_3\text{O}_4\text{-SAS@PLT}$ by flow cytometry.

the system circulation. When the pH value was decreased to 6.5 and 5.5, the SAS release from Fe₃O₄-SAS@PLT was increased to 56.9 ± 4.9% and 79.1 ± 5.0% within 24 h, respectively (Figure S3, Supporting Information). This enhanced release might be partly due to the increased permeability of PLT membrane coating at weak acid environment, which has been reported previously.^[28c] The acidic condition further increased the degradation of magnetic core, triggered the Fe₃O₄-SAS destruction to generate iron ions (Fe²⁺ and Fe³⁺) (Figure S4, Supporting Information) and rapidly release SAS.

2.2. In Vitro Cytotoxicity and Mechanism of Ferroptosis Induced by Fe₃O₄-SAS@PLT

The in vitro cytotoxicity of Fe₃O₄-SAS@PLT toward 4T1 cells was determined by treating 4T1 cells with different concentrations of Fe₃O₄-SAS@PLT. Both Fe₃O₄ and SAS did not display obvious cytotoxicity on 4T1 cells. Intriguingly, both Fe₃O₄-SAS@PLT and Fe₃O₄-SAS reduced cell viability in a dose-dependent manner (Figure 2a), but Fe₃O₄-SAS@PLT demonstrated a lower half maximal inhibitory concentration (IC50) (80.7 μg mL⁻¹ of Fe₃O₄) than Fe₃O₄-SAS (1379 μg mL⁻¹ of Fe₃O₄), suggesting the stronger cytotoxic effect of Fe₃O₄-SAS@PLT than Fe₃O₄-SAS. It has been reported that P-selectin is enriched on the surface of platelet membrane-camouflaged Fe₃O₄-SAS@PLT nanoparticles,^[28b] as demonstrated by western blotting results (Figure 1f). 4T1 cells used in the study were CD44-overexpressing breast cancer cells.^[27b] The higher toxicity of Fe₃O₄-SAS@PLT nanoparticles was probably attributed to the strong affinity between P-selectin of the platelet membrane and CD44 receptors of tumor cells.^[28d] In order to check the higher toxicity of Fe₃O₄-SAS@PLT nanoparticles toward 4T1 cells than naked Fe₃O₄-SAS nanoparticles, we further used inductively coupled plasma spectrometry to determine the cellular uptake of nanoparticles in 4T1 cells quantitatively. It was shown that platelet membrane-camouflaged Fe₃O₄-SAS@PLT nanoparticles showed enhanced cellular uptake in 4T1 cells as compared to that of naked Fe₃O₄-SAS nanoparticles (Figure S5, Supporting Information), indicating that P-selectin and the CD44 receptor interactions contribute to the enhanced cellular uptake of Fe₃O₄-SAS@PLT nanoparticles, thereby generating higher cytotoxicity by ferroptosis.

To explore the mechanism by which Fe₃O₄-SAS@PLT inhibit viability of cancer cells, we further analyzed the possible death modes including apoptosis, necroptosis, autophagy, and ferroptosis^[29] on 4T1 cells caused by Fe₃O₄-SAS@PLT. The apoptosis inhibitor carbobenzoxy-valyl-alanyl-aspartyl-[O-methyl]-fluoromethylketone (z-VAD-FMK), necroptosis inhibitor Necrostatin-1, as well as autophagy inhibitor 3-methyladenine (3-MA) did not improve the viability of Fe₃O₄-SAS@PLT-treated 4T1 cells (Figure S6, Supporting Information), indicating that Fe₃O₄-SAS@PLT did not induce apoptosis, necroptosis, or autophagy in 4T1 cells.

Recently, Stockwell and colleagues have shown that erastin could cause cell death via ferroptosis, with the prominent features of iron-dependence and lipid peroxidation production.^[30,31] Considering Fe₃O₄ could increase iron abundance, which result in Fenton reaction to generate reactive oxygen

species (ROS) and SAS could inhibit cysteine transportation and cause glutathione (GSH) depletion,^[30] we examined the effect of ferroptosis inhibitor ferrostatin-1 (Fer-1) and iron chelator deferoxamine (DFO) on the viability Fe₃O₄-SAS@PLT-treated 4T1 cells, respectively. It was found that both Fer-1 and DFO could significantly decrease Fe₃O₄-SAS@PLT-induced cytotoxicity on 4T1 cells (Figure 2b), suggesting that ferroptosis might be involved in Fe₃O₄-SAS@PLT-induced cell death. Next, the influence of Fe₃O₄-SAS@PLT on the ROS level in 4T1 cells was estimated with the 2,7-dichlorodi-hydrofluorescein diacetate (DCFH-DA) method. The cellular ROS level was significantly elevated in Fe₃O₄-SAS@PLT-treated cells compared with other groups, and importantly, both Fer-1 and DFO significantly downregulated the cellular ROS level in Fe₃O₄-SAS@PLT-treated cells (Figure 2c), indicating ferroptosis occurred in Fe₃O₄-SAS@PLT-treated cells.

Further, the nature of ROS induced by Fe₃O₄-SAS@PLT was identified by flow cytometry using dihydroethidium (DHE, a specific probe for superoxide, O₂⁻), Amplex-Red (a selective probe for hydroxyl radical, H₂O₂), and hydroxyphenyl fluorescein (HPF, a highly sensitive probe for hydroxyl radical, ·OH), respectively. Interestingly, despite dose-dependent increase in total ROS level in Fe₃O₄-SAS@PLT-treated cells, negligible increase was observed in O₂⁻ or H₂O₂ levels with Fe₃O₄-SAS@PLT concentration (Figure 2d). Compared with the control group, Fe₃O₄-SAS@PLT dose-dependently increased the ·OH level in 4T1 cells, almost a fivefold increase at 200 μg mL⁻¹ of Fe₃O₄-SAS@PLT, suggesting that ·OH was probably the main ROS specie in 4T1 cells induced by Fe₃O₄-SAS@PLT. Thereby, we measured the lipid peroxidation of ·OH induction in 4T1 cells with flow cytometry by using C11-BODIPY, a fluorescent probe that detect the lipid peroxidation in live cells. We found that Fe₃O₄-SAS@PLT significantly elevated the lipid peroxidation level in 4T1 cells, while the lipid peroxidation could be greatly inhibited by Fer-1 or DFO (Figure 2e), suggesting the generation of lipid peroxidation by Fe₃O₄-SAS@PLT. In addition, the depletion of cytosolic GSH, which caused by Fe₃O₄-SAS@PLT, could be significantly reduced by Fer-1 or DFO (Figure 2f). The depletion of GSH indicated that the Fe₃O₄-SAS@PLT probably induced ferroptosis via inhibition of glutamate-cystine antiporter system X_c⁻ transporter (XcT) pathway that allows cystine to enter the cells for GSH synthesis. To verify this hypothesis, the expression of system XcT and downstream glutathione peroxidase 4 (GPX4) that could be affected by GSH depletion was determined by western blotting. Fe₃O₄-SAS@PLT treatment significantly down-regulated the system XcT level and the GPX4 level in 4T1 cells (Figure 2g). Intriguingly, this down regulation was reversed after the addition of Fer-1 or DFO, indicating that the system XcT pathway was involved in ferroptosis of Fe₃O₄-SAS@PLT-treated cells.

Since lipid peroxidation was an important functional marker of ferroptosis, lipidomic analysis was performed to study the changes of lipids in 4T1 cells after Fe₃O₄-SAS@PLT treatment, using liquid chromatography-mass spectrometry (Figure 3 and Figure S7, Supporting Information). Untreated 4T1 cells were used as a control. Eighty-four triacylglycerols (TGs), 73 phosphatidylethanolamines (PEs), 72 phosphatidylcholines (PCs), 19 ceramides (Cers), 14 phosphatidylserines (PSs), 11 phosphatidylglycerols (PGs), 8 diacylglycerols (DGs), 8 phosphatidylinositols

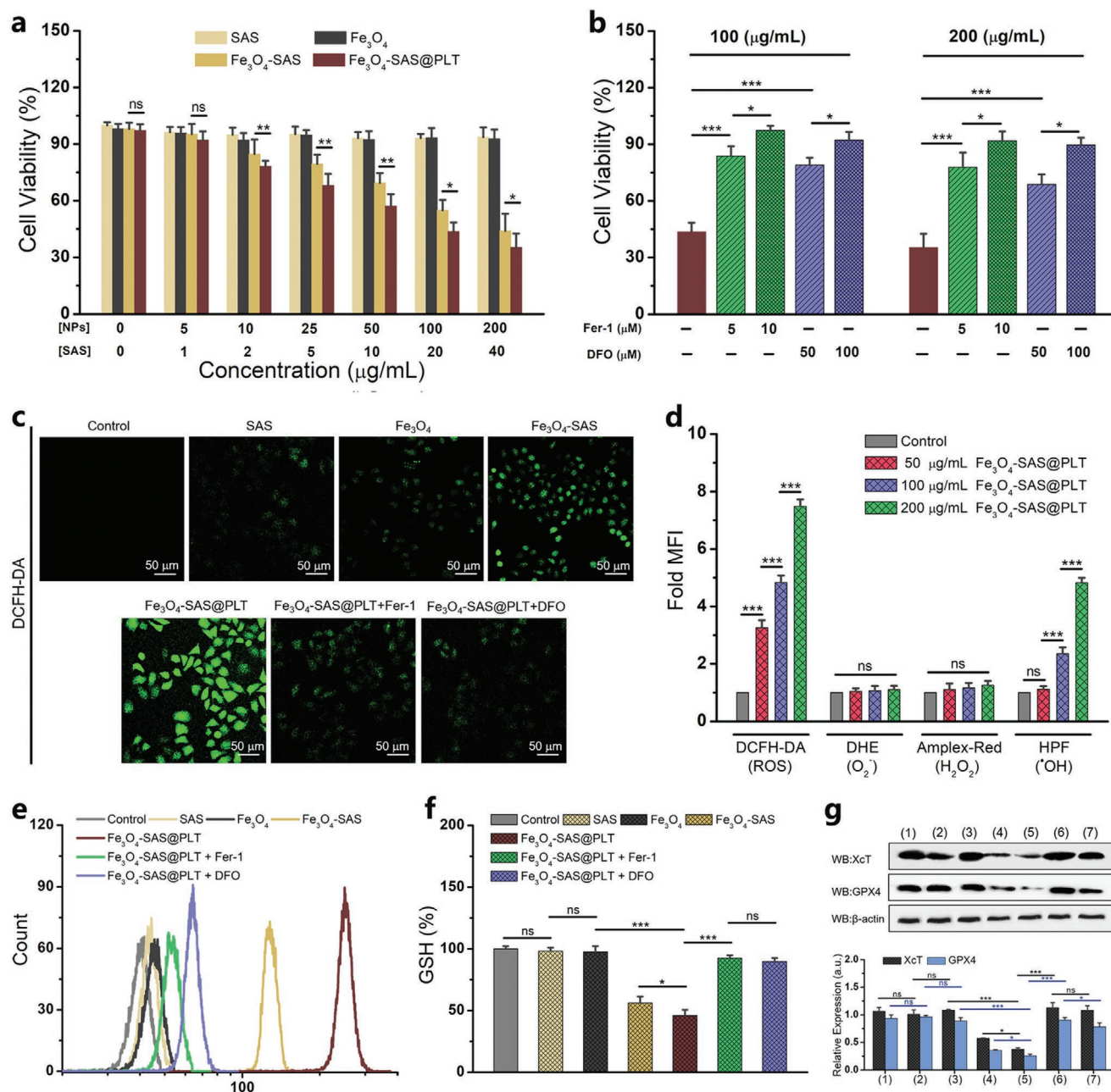


Figure 2. In vitro cytotoxicity and mechanism of ferroptosis induced by Fe₃O₄-SAS@PLT. a) Cell viability of 4T1 cells treated with different concentrations of free SAS, Fe₃O₄, Fe₃O₄-SAS, and Fe₃O₄-SAS@PLT, respectively; *n* = 6. b) Cell viability of Fe₃O₄-SAS@PLT-treated 4T1 cells in the presence of Fer-1 and DFO, respectively; *n* = 6. c) Representative CLSM images of 4T1 cells stained with DCFH-DA in different groups (SAS, Fe₃O₄, Fe₃O₄-SAS, Fe₃O₄-SAS@PLT, Fe₃O₄-SAS@PLT + Fer-1, and Fe₃O₄-SAS@PLT + DFO groups). d) Quantification of total ROS, superoxide, hydroxyl peroxide, and hydroxyl radical by using appropriate fluorescent probes; *n* = 3. e) Flow cytometry analysis of lipid peroxidation in different formulation-treated 4T1 cells by using a C11-BODIPY fluorescent probe. f) Intracellular GSH level in 4T1 cells treated with different formulations (SAS, Fe₃O₄, Fe₃O₄-SAS, Fe₃O₄-SAS@PLT, Fe₃O₄-SAS@PLT + Fer-1, and Fe₃O₄-SAS@PLT + DFO groups); *n* = 3. g) Intracellular XcT and GPX4 expression in 4T1 cells treated with different formulations including 1) Control, 2) SAS, 3) Fe₃O₄, 4) Fe₃O₄-SAS, 5) Fe₃O₄-SAS@PLT, 6) Fe₃O₄-SAS@PLT + Fer-1, and 7) Fe₃O₄-SAS@PLT + DFO; *n* = 3. Untreated 4T1 cells were taken as a control. ns represented no significance, **p* < 0.05, ***p* < 0.01, ****p* < 0.001.

(PIs), 4 sphingosines (Sos), 3 sphingomyelins (SMs), 3 mono-glycerides (MGs), and 1 cardiolipin (CL) were successfully identified and quantified (Figure 3a). The content of several oxygenated polyunsaturated phospholipids was significantly elevated in 4T1 cells after Fe₃O₄-SAS@PLT treatment, suggesting that

the lipid peroxidation occurred (Figure 3b and Figure S8, Supporting Information). The elevation was particularly prominent in the five classes of phospholipids including PE, PC, PG, PS, and PI (Figure 3c). The peroxidized products of PE, PC, and PS were expressed by mono-oxygenation (+10), which might

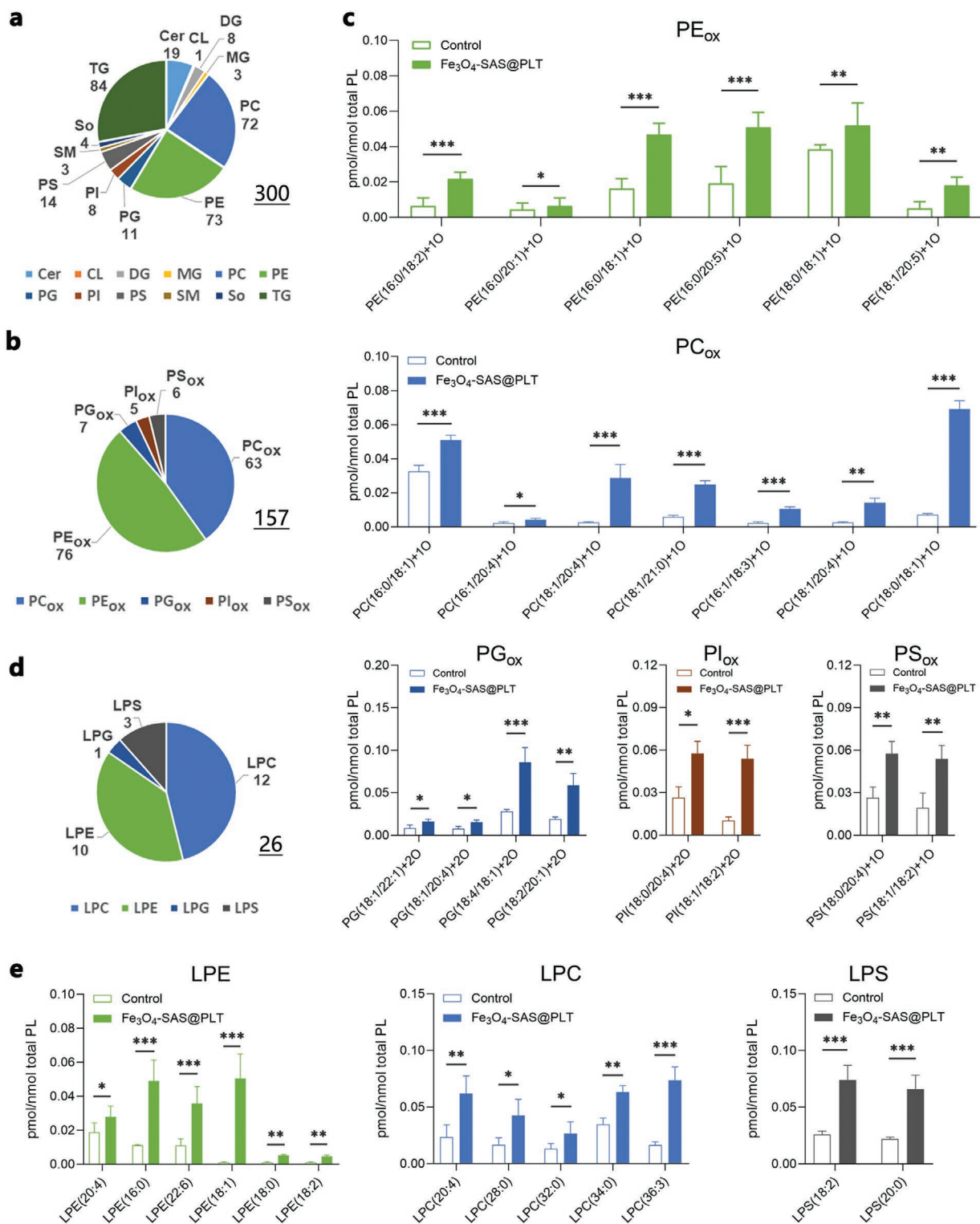


Figure 3. Lipidomics profiles of 4T1 cells treated with Fe₃O₄-SAS@PLT. a) The distribution and number of lipid species in 12 major classes were determined by liquid chromatography-mass spectrometry (LC-MS); Cer, ceramide; CL, cardiolipin; DG, diacylglycerol; MG, monoglyceride; PC, phosphatidylcholine; PE, phosphatidylethanolamine; PG, phosphatidylglycerol; PI, phosphatidylinositol; PS, phosphatidylserine; SM, sphingomyelin; So, sphingosine; TG, triacylglycerol. b) 157 possible oxygenated species of phospholipids (PE_{ox}, PC_{ox}, PG_{ox}, PI_{ox}, and PS_{ox}) were detected and quantified by LC-MS. c) Levels of six mono-oxygenated PEs, seven mono-oxygenated PCs, four di-oxygenated PGs, two di-oxygenated PIs, and two mono-oxygenated PSs in control and Fe₃O₄-SAS@PLT-treated 4T1 cells; data were mean ± SD; *n* = 3. d) Twenty-six species of lyso-phospholipids (LPE, LPC, LPS, and LPG) were detected and quantified by LC-MS. e) Levels of six lyso-PEs, five lyso-PCs, and two lyso-PSs in control and Fe₃O₄-SAS@PLT-treated 4T1 cells; data were mean ± SD; *n* = 3. **p* < 0.05, ***p* < 0.01, ****p* < 0.001.

be hydroxyl derivatives, resulting from reductive metabolism in relation to GPX4.^[31] The oxygenated products of PG and PI were hydroperoxyl content (+2O), which probably attributed to the incomplete reductive metabolism of phospholipid hydroperoxides to the corresponding hydroxyl derivatives.^[32] In addition, levels of several types of lyso-phospholipids such as LPE, LPC, and LPS were elevated significantly in Fe₃O₄-SAS@PLT-treated 4T1 cells compared with those in the control (Figure 3d,e). However, there was no significant elevation of mono-oxygenated or mono-lyso CL species, the high specific products in the execution of intrinsic apoptotic processes^[33] in 4T1 cells after Fe₃O₄-SAS@PLT-treatment. These results corroborated that Fe₃O₄-SAS@PLT induced 4T1 cell death in a caspase-independent manner and with typical lipid peroxidation characteristics, which was consistent with the features of ferroptosis.^[34] Collectively, our results had shown that Fe₃O₄-SAS@PLT-induced cell death was involved in lipid peroxides accumulation, cellular GSH depletion, and system XcT inhibition, indicating that ferroptosis was the main pathway leading to cell death of Fe₃O₄-SAS@PLT-treated 4T1 cells.

2.3. Fe₃O₄-SAS@PLT-Mediated Ferroptosis for In Vitro Immune Activation

After exploring mechanisms of ferroptosis in Fe₃O₄-SAS@PLT-treated tumor cells, whether Fe₃O₄-SAS@PLT-mediated ferroptosis could induce the immune response was investigated in vitro. Dendritic cells (DCs), a specialized system of antigen-presenting cells, are involved in the maintenance of T-cell-mediated immune response.^[35] The immature DCs (iDCs), when exposed to tumor antigens, will engulf and process antigens into peptides. As they move to the surrounding lymphoid tissues, they undergo maturation and show peptide-major histocompatibility complex molecules (MHC-I and MHC-II) to T cells, producing effector T cells to destroy tumors.^[36] Before DC stimulation experiment, we directly treated DCs with various concentrations of SAS, Fe₃O₄, Fe₃O₄-SAS, and Fe₃O₄-SAS@PLT nanoparticles, respectively. It was shown that these nanoformulations did not exert significant cytotoxicity to DCs within the tested concentration range (Figure S9, Supporting Information), suggesting the feasibility of our designed nanoformulations for DC stimulation in vitro. Then, we cocultured Fe₃O₄-SAS@PLT-treated 4T1 cells with iDCs by using a transwell system. 4T1 cells cultured in the upper wells (donor wells), were first incubated with various formulations for 6 h. Afterward, iDCs seeded in the bottom wells (receptor wells) were cocultured with the upper 4T1 cells for another 24 h (Figure 4a). Then, the DCs were collected and subjected to flow cytometry to analyze the expressions of costimulatory molecules CD86 and CD80, which were regarded as the DC maturation markers.^[37] Fe₃O₄-SAS@PLT treatment significantly increased the maturity of DCs (CD86⁺/CD80⁺, gated on CD11c⁺ cells, 82.8%), compared with the control group (1.1%) (Figure 4b,c). In contrast, the addition of ferroptosis inhibitor Fer-1 or DFO significantly demoted the maturation of DCs cocultured with Fe₃O₄-SAS@PLT-treated 4T1 cells (16.9% for Fer-1, 21.0% for DFO, respectively), indicating that Fe₃O₄-SAS@PLT-mediated cell ferroptosis could trigger the effective maturation of DCs. As pristine Fe₃O₄ nanoparti-

cles could also induce ferroptosis in cancer cells,^[17] therefore, even without SAS, some cancer cells co-cultured with pristine Fe₃O₄ nanoparticles were partially died because of the occurrence of ferroptosis (Figure 2a). Therefore, if 4T1 cancer cells after Fe₃O₄ nanoparticle treatment were co-cultured with DCs, they could also slightly promote DC maturation. The secretion of DC activation-related cytokines including TNF- α and interleukin 6 (IL-6),^[38] were also significantly enhanced after DCs were cocultured with Fe₃O₄-SAS@PLT-treated 4T1 cells (Figure 4d), which was consistent with DC maturation. Taken together, these results suggested that cellular immune response was successfully induced by Fe₃O₄-SAS@PLT-mediated tumor cell ferroptosis.

2.4. Fe₃O₄-SAS@PLT-Mediated Ferroptosis for In Vivo Immune System Activation

Recent studies have shown that CD8⁺ T cell could trigger lipid peroxide production and promote the occurrence of ferroptosis, which, in converse, improve the treatment effect of immunotherapy.^[39] Therefore, we wonder whether Fe₃O₄-SAS@PLT, as a new ferroptosis inducer, could induce an immune activation in vivo. Cancer metastasis have been the main challenge for cancer therapy today. Although primary tumors are life-threatening, they would cause only 10% of cancer-related death eventually, and about 90% of patients were died of metastatic growth of tumors beyond of primary lesion.^[40] Platelets play outstanding roles in tumor metastasis because of their recognition and interaction with circulating tumor cells.^[25] Several studies have shown that nanoparticles camouflaged with platelet membranes may not only be effective in eliminating existing metastases, but also be capable of preventing further micrometastasis.^[23–25,41] In our experiment, we established a metastasis model by injecting 4T1-luc cells (2×10^5) into the tail vein of Balb/c mice intravenously. Then, the mice were treated with different formulations (Figure 5a). To verify the occurrence of ferroptosis induced by Fe₃O₄-SAS@PLT in vivo, GPX4 expression in lung metastatic tumor tissues was examined initially (Figure 5b). Compared with other groups (including Control, free SAS, Fe₃O₄, and Fe₃O₄-SAS), the Fe₃O₄-SAS@PLT group showed significantly decreased GPX4 expression in lung metastatic tumors. However, upon the addition of Fer-1 or DFO, the GPX4 expression declination was significantly inhibited, indicating the involvement of ferroptosis in Fe₃O₄-SAS@PLT-treated metastatic tumors.

Next, we collected draining lymph nodes 24 h post-injection (Day 8) and analyzed the maturation of DCs with flow cytometry (Figure 5c). The mature DCs expression, which are CD86⁺/CD80⁺ positive, elaborated significantly in lymphoid nodes of Fe₃O₄-SAS@PLT-treated mice when compared with the free SAS and Fe₃O₄ groups. However, the percentage of mature DCs lymphoid nodes of Fe₃O₄-SAS@PLT-treated mice significantly declined after treatment with Fer-1 or DFO. These results indicated Fe₃O₄-SAS@PLT-mediated ferroptosis improved DC maturation. Specifically, Fe₃O₄-SAS@PLT induced a significant higher maturity of DCs (69.9%) than Fe₃O₄-SAS (28.4%) (Figure 5d), which was probably attributed to the favorable targeting capacity of Fe₃O₄-SAS@PLT to metastatic tumors.

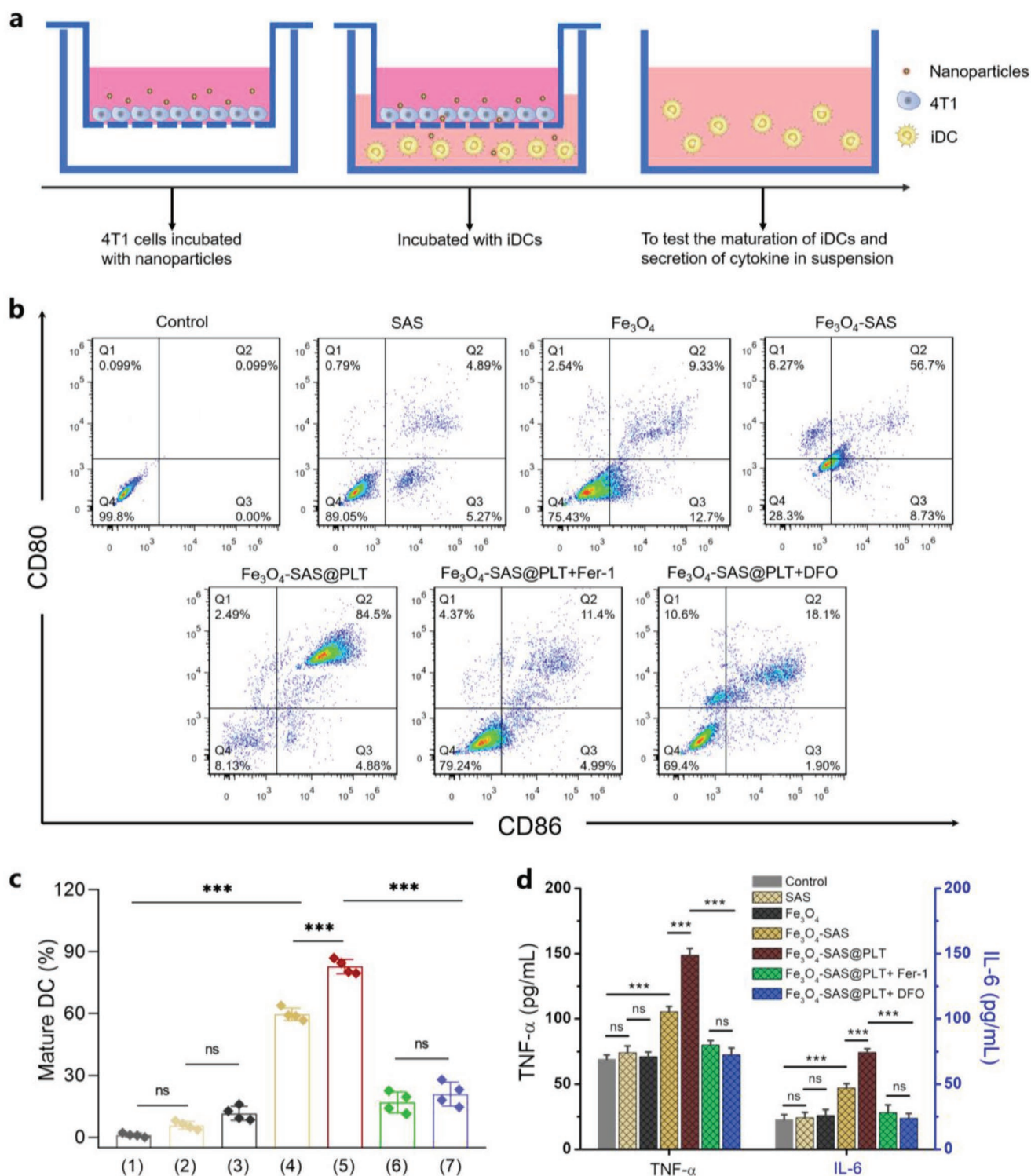


Figure 4. In vitro immune response induced by Fe₃O₄-SAS@PLT. a) Schematic illustration of the coculture system of 4T1 cells and iDCs. b,c) Flow cytometric analysis b) and quantification c) of mature DCs (CD86⁺/CD80⁺, gated on CD11c⁺ cells) at 24 h after various treatments including 1) Control, 2) SAS, 3) Fe₃O₄, 4) Fe₃O₄-SAS, 5) Fe₃O₄-SAS@PLT, 6) Fe₃O₄-SAS@PLT + Fer-1, and 7) Fe₃O₄-SAS@PLT + DFO; untreated 4T1 cells were taken as a control. d) TNF- α and IL-6 secreted in the culture medium by DCs; $n = 4$; ns represented no significance, *** $p < 0.001$.

In addition, we examined various cytokines including TNF- α , IL-6, and interleukin 12 p70 (IL-12p70) in serum from mice at 24, 48, and 72 h (Day 8, 9, and 10) after treatment with various

formulations. The secretion of TNF- α , IL-6 and IL-12p70 in Fe₃O₄-SAS@PLT group significantly elevated at 48 h (on Day 9) after injection compared with other groups (Figure 5e).

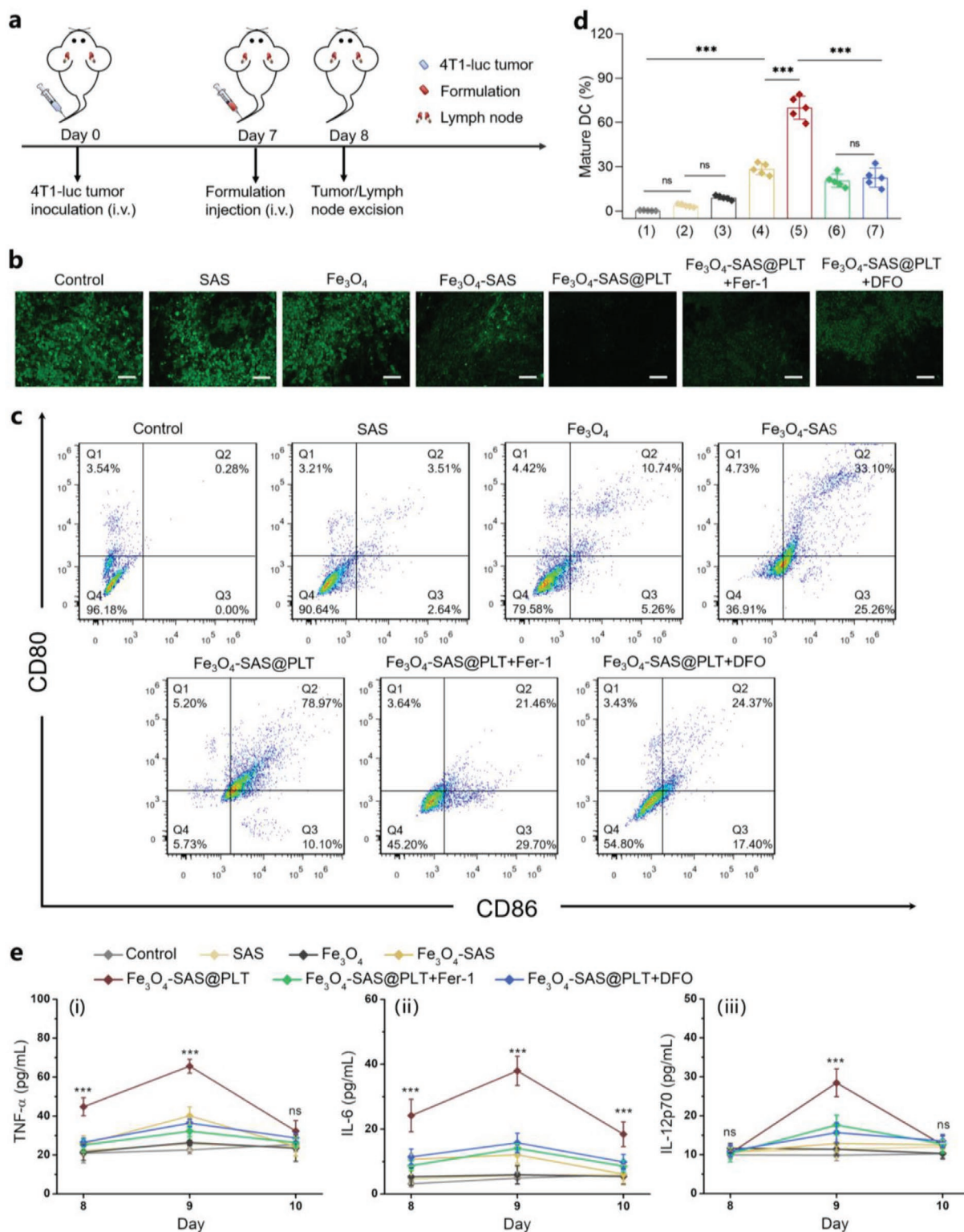


Figure 5. In vivo immune response induced by Fe_3O_4 -SAS@PLT. a) Schematic illustration of dosing regimens of Fe_3O_4 -SAS@PLT in 4T1 metastatic tumor-bearing mice. b) Immunofluorescence images of GPX4 expression in lung metastatic 4T1 tumor tissues at 24 h after mice received different treatments; scale bar: 50 μ m. c) Flow cytometry analysis of mature DCs ($CD86^+/CD80^+$, gated on $CD11c^+$ cells) in the lymph nodes of 4T1 metastatic tumor-bearing mice at 24 h after mice received different treatments. d) Quantification of mature DCs ($CD86^+/CD80^+$, gated on $CD11c^+$ cells) in the lymph nodes of 4T1 metastatic tumor-bearing mice at 24 h after mice received different treatments including 1) Control, 2) SAS, 3) Fe_3O_4 , 4) Fe_3O_4 -SAS, 5) Fe_3O_4 -SAS@PLT, 6) Fe_3O_4 -SAS@PLT + Fer-1, and 7) Fe_3O_4 -SAS@PLT + DFO; untreated 4T1 cells were taken as a control. e) Secretion of TNF- α (i), IL-6 (ii), and IL-12p70 (iii) in serum at 24, 48, and 72 h after mice received different treatments; $n = 5$; ns represented no significance, *** $p < 0.001$.

Meanwhile, this elevation was significantly down-regulated upon the addition of Fer-1 or DFO, suggesting favorable in vivo immune response of Fe₃O₄-SAS@PLT-mediated ferroptosis. Taken together, these results suggested that Fe₃O₄-SAS@PLT-mediated ferroptosis could release tumor-related antigens and trigger effective immune activation in vivo.

2.5. In Vivo Anti-Metastasis Efficacy of Fe₃O₄-SAS@PLT-Mediated Ferroptosis Plus PD-1 Blockade

It has been shown that blocking PD-1/PD-L1 checkpoints promotes antitumor immunity by inhibiting the depletion of effector T cells, particularly after combination with other treatments, greatly improving the antitumor efficacy.^[42] Thereby, we further employed PD-1 blockade to increase the antitumor effect of Fe₃O₄-SAS@PLT-mediated ferroptosis. Before investigating the potential anti-metastatic effect, the circulation and biodistribution of Fe₃O₄-SAS@PLT in 4T1 metastatic tumor-bearing mice were initially evaluated with an inductively couple plasma spectrometer. It revealed that Fe₃O₄-SAS@PLT had a significantly higher accumulation in lung metastatic tumors than Fe₃O₄-SAS after intravenous administration, partly attributing to the longer blood circulation of Fe₃O₄-SAS@PLT than Fe₃O₄-SAS (Figure S10, Supporting Information). The Fe₃O₄-SAS@PLT shown a higher blood retention of 13.0% ID/g than SAS@PLT (2.3% ID/g) at 24 h post-injection, enabling the sustainable accumulation of Fe₃O₄-SAS@PLT in metastatic tumors. It was noteworthy that Fe₃O₄-SAS@PLT had significantly lower hepatic and splenic accumulation than Fe₃O₄-SAS, indicating that Fe₃O₄-SAS@PLT had gained the immune evasion ability after the platelet membrane coating.

Since Fe₃O₄-SAS@PLT showed the ability to target metastatic 4T1 cells in vivo, we further examined the tumor accumulation of Fe₃O₄-SAS@PLT in the metastatic model and monitored it with in vivo imaging. The 4T1 cells expressing firefly luciferase (4T1-luc) was intravenously injected into mice to establish a whole-body metastatic tumor model. Mice then received an intravenous injection of DiD-labeled Fe₃O₄-SAS@PLT for imaging. It was shown that the fluorescence signal of Fe₃O₄-SAS@PLT nanoparticles were clearly observed at tumor sites at 2 h post-injection, and gradually increased with time. The signal of Fe₃O₄-SAS@PLT nanoparticles peaked at 12 h and maintained at a high level at 24 h after injection (Figure S11, Supporting Information), which owned to the long circulation ability and homing ability to metastatic tumors of Fe₃O₄-SAS@PLT. At 24 h post-injection, mice were sacrificed for ex vivo imaging. Mice were injected with D-fluorescein sodium solution at 20 min before sacrifice. Tumor expansion and growth were tracked through the bioluminescence of 4T1-luc cells and the accumulation of Fe₃O₄-SAS@PLT in major organs was detected by the fluorescence intensity of DiD dye. We found that mice showed significant bioluminescence signals in lungs, and almost no bioluminescence signals were observed in other organs, indicating that the lung metastasis of 4T1-luc cells was developed (Figure 6a). Fluorescence imaging and the corresponding semi-quantitative results showed that Fe₃O₄-SAS@PLT had higher enrichment in the liver, spleen, and lung than that in other organs and the enrichment in the liver, spleen,

and lung was not significantly different (Figure 6b), indicative of outstanding metastasis targeting of Fe₃O₄-SAS@PLT in vivo. Furthermore, we carefully tracked the accumulation of FeO₄-SAS@PLT in metastatic tumor with in vivo imaging.

Next, to assess the potency of the combined Fe₃O₄-SAS@PLT-mediated ferroptosis/immunotherapy strategy, the 4T1-luc metastatic tumor bearing-mice received different treatments as described in Figure 6c. Considering the blood-circulation duration of Fe₃O₄-SAS@PLT and high aggressiveness of lung metastasis, multiple dosing of Fe₃O₄-SAS@PLT and anti-PD-1 antibody was applied. Mice were intravenously injected with Fe₃O₄-SAS@PLT and anti-PD-1 antibody on Day 7, 9, 11, and 13. The bioluminescence of 4T1-luc cells was recorded to monitor the tumor metastasis expansion and growth (Figure 6d). Bioluminescence imaging showed that tumor cells had clearly spread to the lung at Day 7 after mice received 4T1-luc cell injection. There was observation of a weaker bioluminescence increment in the mice of groups of free SAS, Fe₃O₄, or Fe₃O₄-SAS nanoparticles, compared to that of control group, while tumor metastases in the mice treated alone with Fe₃O₄-SAS@PLT or anti-PD-1 antibody were observed until the 21st day (Figure 6e). In contrast, mice treated with Fe₃O₄-SAS@PLT + anti-PD-1 showed nearly no metastasis, indicating that tumor metastasis were substantially suppressed. The lung from each group was collected on the 28th day, photographed after Bouin's staining, and numbers of metastatic nodules in the lung were recorded (Figure 6f). Very few metastatic nodules were observed in the lunge of the Fe₃O₄-SAS@PLT + anti-PD-1 group (1.8 ± 1.4), and it was significantly less than with that of the control group (48.6 ± 13.2). It was found that 76% of mice treated with Fe₃O₄-SAS@PLT + anti-PD-1 survived in 80 days. In stark contrast, all mice in other groups died in 50 days (Figure 6g). Pathological slices revealed that the lung in the control group was occupied by tumor metastasis while almost no metastatic nodules were found in the lung of the Fe₃O₄-SAS@PLT + anti-PD-1 group (Figure 6h), suggesting the effectiveness of this combined treatment strategy (Fe₃O₄-SAS@PLT-mediated ferroptosis plus anti-PD-1 therapy) for anti-lung metastasis. Taken together, these results suggested that a joint therapy of PD-1 blockade and Fe₃O₄-SAS@PLT-mediated ferroptosis inhibited tumor metastasis, providing a remarkable advantage in extending survival of metastatic tumor-bearing mice.

2.6. Mechanism Study of Fe₃O₄-SAS@PLT-Mediated Ferroptosis Enhancing Cancer Immunotherapy

To understand the mechanism of Fe₃O₄-SAS@PLT-mediated ferroptosis enhancing anti-tumor immune response, a tandem mass tags (TMT)-based proteomic analysis was performed on tumors before (Control group) and after Fe₃O₄-SAS@PLT treatment (Fe₃O₄-SAS@PLT group). The analysis of protein levels through a proteomic method could provide a better characterization of pathophysiological alternation in a diseased tissue.^[43] We have identified 4753 trusted proteins, 2833 of which were selected as reliable proteins with unique peptide ≥ 2 (Table S1, Supporting Information). Based on these reliable proteins, we carried out principle component analysis (PCA) to highlight any similarities or differences between samples (Figure S12,

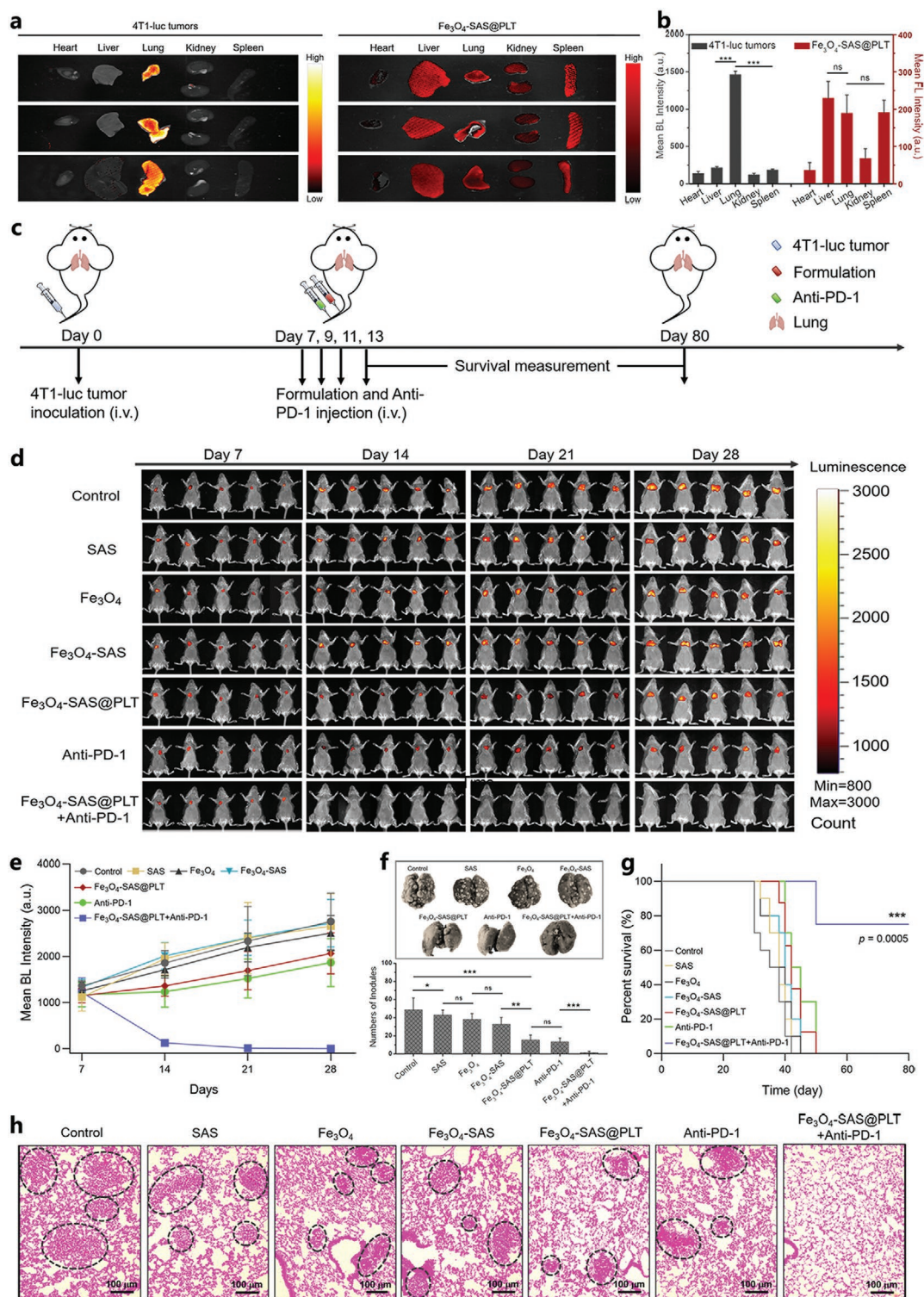


Figure 6. Anti-metastatic tumor effect of $\text{Fe}_3\text{O}_4\text{-SAS@PLT}$ -mediated ferroptosis plus anti-PD-1 immunotherapy in 4T1 metastatic tumor-bearing mice. a) Ex vivo bioluminescence imaging (left) and fluorescence imaging (right) of major organs 24 h post-injection of $\text{Fe}_3\text{O}_4\text{-SAS@PLT}$. b) Bioluminescence intensity of 4T1-luc tumor cells and fluorescence intensity of $\text{Fe}_3\text{O}_4\text{-SAS@PLT}$ in different organs; $n = 3$; ns represented no significance, *** $p < 0.001$. c) Schematic illustration of dosing regimens of $\text{Fe}_3\text{O}_4\text{-SAS@PLT}$ -mediated ferroptosis combined with anti-PD-1 immunotherapy in 4T1-luc metastatic tumor models. d) In vivo bioluminescence images of mice in different groups; $n = 5$. e) Quantification of bioluminescence intensity of mice in different groups; $n = 5$; *** $p < 0.001$ compared with any other group. f) Representative lung photographs and number of lung metastasis nodules in different groups; $n = 5$; ns represented no significance, * $p < 0.05$, ** $p < 0.01$, *** $p < 0.001$. g) Survival curves of mice in different groups in 80 days; $n = 10$. h) Representative H&E-images of lung tissues in different groups; scale bar = 100 μm .

Supporting Information). PCA result revealed a clear separation between Control group and Fe₃O₄-SAS@PLT group, suggesting the dynamic change of the protein expression in response to Fe₃O₄-SAS@PLT treatment. Changes of reliable proteins greater than 1.2 and a *p*-value less than 0.05 were considered differential expressions. The total number of differentially expressed proteins was 271 (Figure S13 and Table S2, Supporting Information)

and the differential expressions were reflected by a clustering heat map (Figure S14, Supporting Information). First, we focused on differential protein expression related to ferroptosis. Fe₃O₄-SAS@PLT significantly reduced the expression of solute carrier family member 2 (Slc3a2) and solute carrier family 12 member 7 (Slc12a7) (Figure 7a). It has been reported that Slc3a2 is involved in the exchange process of extracellular cystine and

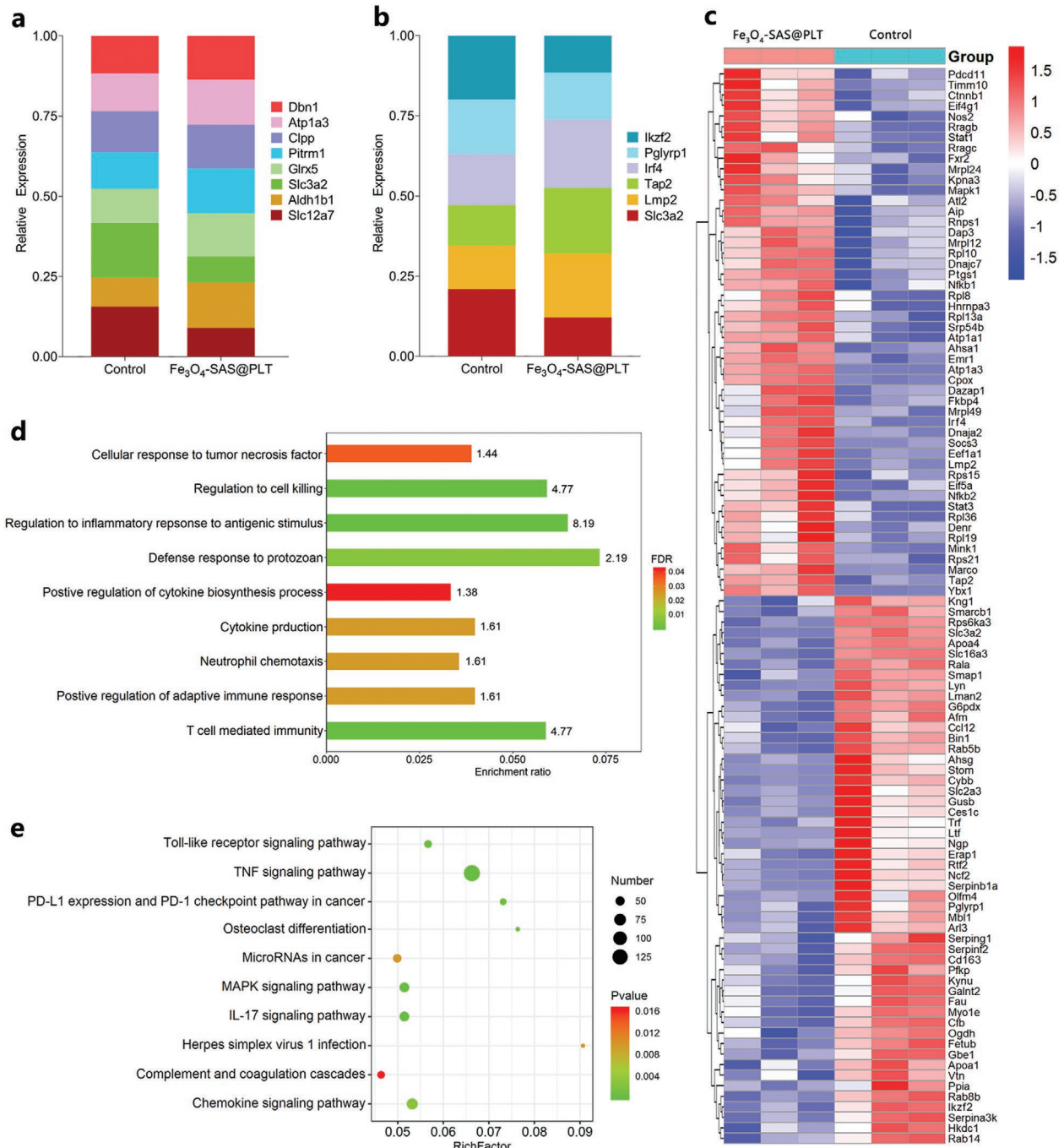


Figure 7. Mechanism of Fe₃O₄-SAS@PLT-mediated ferroptosis enhancing anti-tumor immune response. a) Relative change of differentially expressed protein expression related to Fe₃O₄-SAS@PLT-mediated ferroptosis. b) Relative change of differentially expressed protein expression associated with the activation of CD8⁺ and CD4⁺ effector T cells. c) The heat map of differentially expressed proteins related to immune functions. d,e) GO enrichment analysis d) and KEGG pathway enrichment analysis e) of differentially expressed proteins involved in immune processes.

intracellular glutamate, which is an important component of system X_c^- transporter.^[44] The down-regulation of Slc3a2 confirmed that Fe₃O₄-SAS@PLT induced ferroptosis by inhibiting XcT pathway and reducing the uptake of cystine.

Second, we quantified the differential protein expression associated with ferroptosis-activated T cell activation and infiltration (mainly CD8⁺ and CD4⁺ effector T cells), which have a very close relationship with PD-1 treatment.^[45] In tumor tissue treated with Fe₃O₄-SAS@PLT, Slc3a2 expression was low, whereas low molecular mass polypeptide (Lmp2) and transporter associated with antigen presentation 2 (Tap2) was highly expressed on tumors (Figure 7b), indicating that tumor tissues were highly infiltrated by CD8⁺ effector T cells.^[39,46] There was also a significant difference in the expression of CD4⁺ effector T cell-related proteins in tumor tissues between the two groups. High expression of interferon regulatory factor 4 (Irf4) and low expression of peptidoglycan recognition protein 1 (Pglyrp1) or Ikaros family zinc finger protein 2 (Ikzf2) in the Fe₃O₄-SAS@PLT group were positively correlated with CD4⁺ effector T cell signature,^[47] indicating Fe₃O₄-SAS@PLT treatment activated CD4⁺ effector T cells in tumor tissues. Taken together, these results suggested that Fe₃O₄-SAS@PLT-mediated ferroptosis could activate DC maturation, T cells activation and infiltration, thus promoting PD-1 treatment.

Next, we focused on proteins related to immune functions to better understand how Fe₃O₄-SAS@PLT promoted anti-tumor immune response. We found a total of 102 differential expressed proteins were involved, of which 50 protein expressions were up-regulated and 52 protein expressions were down-regulated. The heat map of those proteins was shown in Figure 7c. Pathway analysis based on Gene Ontology (GO) process showed that these 102 differentially expressed proteins enriched significantly in immune processes, particularly involved in regulation to cell killing, regulation to inflammatory to antigenic stimulus, defense response to protozoan, T cell mediated immunity, and so on (Figure 7d), indicating that specific immune pathways associated with antitumor response were activated after Fe₃O₄-SAS@PLT treatment. Among the protein sets, Kyoto Encyclopedia of Genes and Genomes (KEGG) pathway analysis indicated that the most represented processes included tumor necrosis factor (TNF) signaling pathway, mitogen-activated protein kinase (MAPK) signaling pathway, interleukin 17 (IL-17) signaling pathway, and chemokine signaling pathway (Figure 7e), which are important pathways of immune system activation.^[48] Particularly, in the protein sets belonged to MAPK signaling pathway, we found that the nuclear factor NF-kappa-B family proteins (Nfkb1 and Nfkb2), which play a key role in promoting M1 polarization,^[49] significantly upregulated in response to Fe₃O₄-SAS@PLT treatment, suggesting that Fe₃O₄-SAS@PLT treatment might repolarize immunosuppressive M2 macrophages toward the antitumor M1 phenotype.

Moreover, among the proteins associated with immune response processes, several typical markers of macrophage polarization toward the alternatively activated M1 phenotypes^[16,50] such as signal transducer and transcription activator 1 (Stat1), signal transducer and transcription activator 3 (Stat3), nitric oxide synthase 2 (Nos2), and prostaglandin-endoperoxide synthase 2 (Ptgs2), were over represented in the

tumors of Fe₃O₄-SAS@PLT-treated mice (Table S3, Supporting Information), suggesting the accumulation of M1-polarized macrophages in tumors. Notably, it was reported previously that the induction of ferroptosis and the inactivation of GPX4 could promote the sustainable release of Ptg2.^[51] The overexpression of Ptg2 protein in Fe₃O₄-SAS@PLT group was noticeable, which indirectly verified the occurrence of ferroptosis induced by Fe₃O₄-SAS@PLT in vivo.

Furthermore, we explored whether Fe₃O₄-SAS@PLT nanoparticles could repolarize M2 macrophages to M1 phenotype by using flow cytometry. First, we preincubated RAW264.7 macrophages with interleukin 4 for 24 h to polarize the macrophages to the M2 state. Then, we incubated macrophages with Fe₃O₄-SAS@PLT nanoparticles for another 24 h (designed as Fe₃O₄-SAS@PLT group). The macrophages without Fe₃O₄-SAS@PLT nanoparticle treatment were used as the control (Control group). After that, cells were harvested and the populations of M1 phenotype (CD86⁺/CD80⁺, gated on CD11c⁺ cells) and M2 phenotype (CD206⁺, gated on CD11c⁺ cells) were analyzed by flow cytometry. It was shown that Fe₃O₄-SAS@PLT treatment resulted in a remarkable increase in M1-type macrophages and a decrease in M2-type macrophages, as compared with that of the control group (Figure S15, Supporting Information), suggesting macrophages polarized from M2 phenotype to M1 phenotype. At the same time, enzyme-linked immunosorbent assay revealed that the levels of antitumor inflammatory cytokines TNF- α , IL-6, and IL-12p70 in the supernatants of Fe₃O₄-SAS@PLT-treated RAW264.7 macrophages increased 2 to 56 times (Figure S16a–c, Supporting Information). In addition, NO production was significantly increased in the Fe₃O₄-SAS@PLT groups (Figure S16d, Supporting Information), consistent with the upregulation of marker of M1 macrophages of nitric oxide synthase 2 investigated by proteomics analysis (Table S3, Supporting Information). Collectively, these results successfully demonstrate that our findings on the Fe₃O₄-SAS@PLT nanoparticles could polarize M2 phenotype macrophages to M1 phenotype, promoting antitumor immune response effectively.

3. Conclusion

In summary, a biomimetic magnetic nanopatform (Fe₃O₄-SAS@PLT) has been developed to sensitize effective ferroptosis and improve cancer immunotherapy. Owing to the self-recognition feature of platelet membranes, Fe₃O₄-SAS@PLT show effective immune evasion and sufficient enrichment in tumor metastasis. It was found that Fe₃O₄-SAS@PLT could not only effectively trigger ferroptosis of tumor cells through the inhibition of glutamate-cystine antiporter system X_c^- transporter pathway, but also induce an effective immune response for enhancing the therapeutic efficacy of PD-1 blockade in vivo. The Fe₃O₄-SAS@PLT-mediated ferroptosis jointly with immunotherapy effectively inhibited the metastasis tumor growth compared with single therapies. In addition, proteomic analysis revealed that Fe₃O₄-SAS@PLT-mediated ferroptosis could repolarize macrophages from immunosuppressive M2 phenotype to antitumor M1 phenotype. Collectively, accompanied by repolarization of tumor-associated macrophages, Fe₃O₄-SAS@PLT-mediated ferroptosis could reinforce systemic antitumor

immunity, which provides a new way of clinically applicable synergistic immunotherapy in cancer. Considering that the main components within the designed $\text{Fe}_3\text{O}_4\text{-SAS@PLT}$ nanoparticles have excellent biocompatibility and biosafety, this therapeutic modality is expected to be promising in combating cancer.

4. Experimental Section

Preparation of $\text{Fe}_3\text{O}_4\text{-SAS@PLT}$: Briefly, $\text{Fe}_3\text{O}_4\text{-SAS}$ (3.5 mg mL^{-1} , calculated as Fe_3O_4 concentration, $100 \mu\text{L}$) was mixed with the PLT membrane suspension (1 mg mL^{-1} , calculated as the membrane protein concentration, $150 \mu\text{L}$). The preparation of Fe_3O_4 , $\text{Fe}_3\text{O}_4\text{-SAS}$, and PLT membrane-derived vesicles is described in the Supporting Information. The mixture was diluted to $400 \mu\text{L}$ and membrane fusion was facilitated by continuous extrusion process. Then, $\text{Fe}_3\text{O}_4\text{-SAS@PLT}$ were separated by using a magnet and washed three times with PBS to remove excessive PLT membranes. To prepare DiD dye-labeled $\text{Fe}_3\text{O}_4\text{-SAS@PLT}$, DiD dye was first labeled to PLT membranes before their fusion with $\text{Fe}_3\text{O}_4\text{-SAS}$. PLT membranes (1 mg mL^{-1} , $150 \mu\text{L}$) were mixed with DiD dye (1 mg mL^{-1} , $15 \mu\text{L}$, in DMSO) for 2 h in the dark. The excessive dye was removed by centrifugation for 30 min at $21\,000 \times g$, 4°C , followed by washing three times with PBS. The loading amount of DiD was calculated to be 1% (DiD/ $\text{Fe}_3\text{O}_4\text{-SAS@PLT}$, m/m).

In Vitro Cytotoxicity Assay and Cellular Uptake: CCK-8 assay was used for evaluating the cytotoxicity of $\text{Fe}_3\text{O}_4\text{-SAS@PLT}$ against 4T1 cells. First, 4T1 cells were seeded with 1×10^4 cells per well in 96-well plates. After cells reached 70–80% confluence, cells were treated with different concentrations of $\text{Fe}_3\text{O}_4\text{-SAS@PLT}$ (0, 5, 10, 25, 50, 100, and $200 \mu\text{g mL}^{-1}$, considered as the Fe_3O_4 concentration) for 24 h, followed by determining the cell viability with CCK-8 method. An Epoch2 microplate spectrophotometer (BioTek, USA) was used to read the absorbance at 450 nm. Free SAS, Fe_3O_4 , and $\text{Fe}_3\text{O}_4\text{-SAS}$ formulations at equivalent concentrations were used as the controls. To evaluate the cellular uptake of $\text{Fe}_3\text{O}_4\text{-SAS@PLT}$ nanoparticles, 4T1 cells were seeded with 1×10^6 cells per well in 35 mm glass-bottomed dishes. After cells reached 70–80% confluence, cells were treated with $\text{Fe}_3\text{O}_4\text{-SAS@PLT}$ nanoparticles ($200 \mu\text{g mL}^{-1}$) for different times (2, 4, 6, 8, 10, 12, 14, 16, 18, and 24 h), the cells were digested, centrifuged, harvested, lysed, and subjected to Fe concentration determination. The naked $\text{Fe}_3\text{O}_4\text{-SAS}$ nanoparticles with same concentration were used as the control. Experiments were performed in triplicate.

Assessment of Ferroptosis: To investigate the modality of $\text{Fe}_3\text{O}_4\text{-SAS@PLT}$ -induced cell death, the cell viability of $\text{Fe}_3\text{O}_4\text{-SAS@PLT}$ -treated 4T1 cells upon the addition of apoptosis inhibitor z-VAD-FMK, necroptosis inhibitor Necrostatin-1, autophagy inhibitor 3-MA, ferroptosis inhibitor ferrostatin-1 (Fer-1), or iron chelator deferoxamine (DFO), was determined. Briefly, 1×10^4 4T1 cells per well were seeded in the 96-well plates. After reaching 70–80% confluence, cells were incubated with $\text{Fe}_3\text{O}_4\text{-SAS@PLT}$ (100 and $200 \mu\text{g mL}^{-1}$) in the presence of Fer-1 ($5 \mu\text{M}$, $10 \mu\text{M}$), DFO ($50 \mu\text{M}$, $100 \mu\text{M}$), z-VAD-FMK ($10 \mu\text{M}$), Necrostatin-1 ($10 \mu\text{M}$), or 3-MA ($10 \mu\text{M}$) for 24 h. Afterward, the cell viability was determined with CCK-8 method.

Intracellular Lipid Peroxide Measurement: A C11-BODIPY 581/591 probe, which could indicate the existence of intracellular lipid peroxide, was used to investigate the production of lipid peroxide in $\text{Fe}_3\text{O}_4\text{-SAS@PLT}$ -treated 4T1 cells. Briefly, 1×10^4 cells per well were seeded in the 96-well plates. After reaching 70–80% confluence, cells were incubated with $\text{Fe}_3\text{O}_4\text{-SAS@PLT}$ ($200 \mu\text{g mL}^{-1}$) in the presence of Fer-1 ($10 \mu\text{M}$) or DFO ($100 \mu\text{M}$) for 6 h. After removing the medium, cells were washed with PBS for three times, and stained with C11-BODIPY ($10 \mu\text{M}$, in free medium) for 20 min. After washing with PBS for three times, cells were collected and subjected to flow cytometry. 4T1 cells treated with free SAS, Fe_3O_4 , and $\text{Fe}_3\text{O}_4\text{-SAS}$ formulations with the equivalent Fe_3O_4 or SAS concentration were used as the controls.

In Vitro DC Stimulation Experiment: Bone marrow-derived dendritic cells (DCs) were isolated from Balb/c mice aged from 6 to 8 weeks

by using a previously published method.^[5] To study the potential cytotoxicity of nanoformulations, DCs were seeded with 1×10^4 cells per well in the 96-well plates. After cells reached 70–80% confluence, DCs were incubated with various concentrations of $\text{Fe}_3\text{O}_4\text{-SAS@PLT}$ (0, 5, 10, 25, 50, 100, and $200 \mu\text{g mL}^{-1}$) for 24 h, followed by determining the cell viability with CCK-8 method. Free SAS, Fe_3O_4 , and $\text{Fe}_3\text{O}_4\text{-SAS}$ formulations at equivalent concentrations were used as the controls. Experiments were performed in quadruplicate. The in vitro DC stimulation experiment was conducted in a 24-well transwell system with $0.4\text{-}\mu\text{m}$ polycarbonate porous membranes. Briefly, 1×10^4 4T1 cells per well were seeded in the upper wells of this system. After reaching 70–80% confluence, cells were incubated with $\text{Fe}_3\text{O}_4\text{-SAS@PLT}$ ($200 \mu\text{g mL}^{-1}$) in the presence of Fer-1 ($10 \mu\text{M}$) or DFO ($100 \mu\text{M}$) for 6 h. Afterward, the upper wells were transferred and coincubated with DCs which were seeded in the bottom wells at a density of 5×10^4 cells per well. 4T1 cells treated with free SAS, Fe_3O_4 , and $\text{Fe}_3\text{O}_4\text{-SAS}$ formulations with the equivalent Fe_3O_4 or SAS concentration were used as the controls. After coincubation, DCs were collected and stained with $5 \mu\text{L}$ of anti-CD11c FITC (eBioscience, 0.2 mg mL^{-1}), $5 \mu\text{L}$ of anti-CD86 PE (eBioscience, 0.2 mg mL^{-1}), and $5 \mu\text{L}$ of anti-CD80 APC (eBioscience, 0.2 mg mL^{-1}) for 15 min. After centrifugation for 5 min at $120 \times g$, DCs were resuspended and analyzed with flow cytometry. After various treatments, the secretion of cytokines including TNF- α and IL-6 in the supernatant of DCs was quantified by enzyme-linked immunosorbent assay kits (ELISA, Invitrogen) under the guidance of manufacturer's instructions.

In Vivo Immune Stimulation Experiment: For in vivo immune stimulation study, each female Balb/c mouse aged from 6 to 8 weeks (BK, Shanghai) was injected with 2×10^5 4T1-luc cells via the tail vein and the day for cell injection was regarded as Day 0. After the metastasis model establishment (Day 7), mice were randomly divided into seven groups ($n = 5$) and respectively received different treatments: 1) Control, 2) SAS ($400 \mu\text{g mL}^{-1}$, $100 \mu\text{L}$), 3) Fe_3O_4 (2 mg mL^{-1} , $100 \mu\text{L}$), 4) $\text{Fe}_3\text{O}_4\text{-SAS}$ (2 mg mL^{-1} , $100 \mu\text{L}$), 5) $\text{Fe}_3\text{O}_4\text{-SAS@PLT}$ (2 mg mL^{-1} , $100 \mu\text{L}$), 6) $\text{Fe}_3\text{O}_4\text{-SAS@PLT}$ (2 mg mL^{-1} , $100 \mu\text{L}$) + Fer-1 ($10 \mu\text{M}$, $100 \mu\text{L}$), 7) $\text{Fe}_3\text{O}_4\text{-SAS@PLT}$ (2 mg mL^{-1} , $100 \mu\text{L}$) + DFO ($100 \mu\text{M}$, $100 \mu\text{L}$). All formulations were administrated intravenously via the tail vein. At 24 h after administration, mice were sacrificed. The lymphoid nodes were collected, cut into pieces, homogenized with $1 \times$ PBS containing 2% FBS to prepare single cell suspensions. For assessing the DCs maturation, single cell suspensions were stained with anti-CD11c FITC, anti-CD86 PE, and anti-CD80 APC antibodies as described above, and analyzed with flow cytometry. In addition, 24 h (Day 8), 48 h (Day 9), and 72 h (Day 10) post-injection, the serum of mice in different groups was collected and the secretion levels of cytokines were determined including TNF- α , IL-6, and IL-12p70 by ELISA kits.

$\text{Fe}_3\text{O}_4\text{-SAS@PLT}$ -Mediated Ferroptosis and PD-1 Blockade for Anti-Metastasis Treatment: After metastasis model establishment (Day 7), mice were randomly divided into seven groups ($n = 5$) and received different treatments on Day 7, 9, 11, and 13, respectively: 1) Control, 2) SAS ($400 \mu\text{g mL}^{-1}$, $100 \mu\text{L}$), 3) Fe_3O_4 (2 mg mL^{-1} , $100 \mu\text{L}$), 4) $\text{Fe}_3\text{O}_4\text{-SAS}$ (2 mg mL^{-1} , $100 \mu\text{L}$), 5) $\text{Fe}_3\text{O}_4\text{-SAS@PLT}$ (2 mg mL^{-1} , $100 \mu\text{L}$), 6) Anti-PD-1 ($20 \mu\text{g mL}^{-1}$, $100 \mu\text{L}$), 7) $\text{Fe}_3\text{O}_4\text{-SAS@PLT}$ (2 mg mL^{-1} , $100 \mu\text{L}$) + Anti-PD-1 ($20 \mu\text{g mL}^{-1}$, $100 \mu\text{L}$). The bioluminescence of mice was recorded with an In-Vivo Xtreme imaging system (Bruker, USA) on Day 7, 14, 21, and 28, respectively. Each mouse received D-Luciferin sodium solution ($150 \mu\text{g mL}^{-1}$, $100 \mu\text{L}$, i.v.) at 20 min before bioluminescence imaging. At the end of study, mice were sacrificed. The lungs were collected, stained with Bouin's solution (Servicebio, China), and photographed. The metastatic tumor modules in the lungs were enumerated by using a BX43 microscope (Olympus, Japan). The lung tissues were also sliced and stained with hematoxylin and eosin (H&E) for histological analysis.

Statistics: The data were presented as mean \pm SD values from at least triplicate experiments. Statistical analyses were performed by either unpaired Student's *t*-test or one way-analysis of variance using GraphPad Prism 8 software. The statistical significance of differences was set at $p < 0.05$.

Study Approval: All animal experiments were conducted in accordance with the Guidelines for the Care and Use of Experimental Animals in Fudan University and the study protocols were evaluated and approved by the Ethics Committee of Fudan University.

Supporting Information

Supporting Information is available from the Wiley Online Library or from the author.

Acknowledgements

This work was supported by the National Science Foundation of China (Grant Nos. 51933002, 51873041, and 81773283) and the National Key R&D Program of China (Grant No. 2016YFC1100300). The authors deeply thank Meigui Zhu and the teamwork (Bionovogene Co., Ltd., Suzhou, China) for lipidomics and proteomics characterization. Especially, author Q.J. would like to express deepest thanks to Dr. Yao Zhao and Dr. Zhenwen Zhao (Institute of Chemistry, Chinese Academy of Sciences, Beijing, China) for their professional analysis and helpful discussion in lipidomics and proteomics.

Conflict of Interest

The authors declare no conflict of interest.

Keywords

ferroptosis, immunotherapy, macrophage repolarization, magnetic nanoparticles, platelet membrane

Received: March 15, 2020

Published online:

- [1] D. S. Chen, I. Mellman, *Immunity* **2013**, *39*, 1.
- [2] S. Matsueda, D. Y. Graham, *World J. Gastroenterol.* **2014**, *20*, 1657.
- [3] J. R. Brahmer, S. S. Tykodi, L. Q. Chow, W. Hwu, S. L. Topalian, P. Hwu, C. G. Drake, L. H. Camacho, J. Kauh, K. Odunsi, *N. Engl. J. Med.* **2012**, *366*, 2455.
- [4] a) G. X. Lan, K. Y. Ni, Z. W. Xu, S. S. Veroneau, Y. Song, W. B. Lin, *J. Am. Chem. Soc.* **2018**, *140*, 5670; b) J. Ouyang, L. Q. Wang, W. S. Chen, K. Zeng, Y. J. Han, Y. Xu, Q. F. Xu, L. Deng, Y. N. Liu, *Chem. Commun.* **2018**, *54*, 3468; c) H. Phuengkham, L. Ren, I. W. Shin, Y. T. Lim, *Adv. Mater.* **2019**, *31*, 1803322; d) M. Wen, J. Ouyang, C. W. Wei, H. Li, W. S. Chen, Y. N. Liu, *Angew. Chem., Int. Ed.* **2019**, *58*, 17425;
- [5] Q. Chen, L. G. Xu, C. Liang, C. Wang, R. Peng, Z. Liu, *Nat. Commun.* **2016**, *7*, 13193.
- [6] J. Xu, L. G. Xu, C. Y. Wang, R. Yang, Q. Zhuang, X. Han, Z. L. Dong, W. W. Zhu, R. Peng, Z. Liu, *ACS Nano* **2017**, *11*, 4463.
- [7] X. Y. Ye, X. Liang, Q. Chen, Q. W. Miao, X. L. Chen, X. D. Zhang, L. Mei, *ACS Nano* **2019**, *13*, 2956.
- [8] L. Sagiv-Barfi, D. K. Czerwinski, S. Levy, I. S. Alam, A. T. Mayer, S. S. Gambhir, R. Levy, *Sci. Transl. Med.* **2018**, *10*, eaan4488.
- [9] M. J. Mosquera, S. W. Kim, H. Zhou, T. T. Jing, M. Luna, J. D. Guss, P. Reddy, K. Lai, C. A. Leifer, I. L. Brito, C. J. Hernandez, A. Singh, *Sci. Adv.* **2019**, *5*, eaav9788.
- [10] a) Z. J. Zhou, J. B. Song, R. Tian, Z. Yang, G. C. Yu, L. S. Lin, G. F. Zhang, W. P. Fan, F. W. Zhang, G. Niu, L. M. Nie, X. Y. Chen, *Angew. Chem., Int. Ed.* **2017**, *56*, 6492; b) J. C. Li, X. Zhen, Y. Lyu, Y. Y. Jiang, J. G. Huang, K. Y. Pu, *ACS Nano* **2018**, *12*, 8520.
- [11] a) R. Liu, M. N. Yu, X. T. Yang, C. S. Umeshappa, C. Hu, W. Q. Yu, L. Qin, Y. Huang, H. L. Gao, *Adv. Funct. Mater.* **2019**, *29*, 1808462; b) X. Zhen, C. Xie, Y. Y. Jiang, X. Z. Ai, B. G. Xing, K. Y. Pu, *Nano Lett.* **2018**, *18*, 1498.
- [12] S. J. Dixon, K. M. Lemberg, M. R. Lamprecht, R. Skouta, E. M. Zaitsev, C. E. Gleason, D. N. Patel, A. J. Bauer, A. M. Cantley, W. S. Yang, B. Morrison III, B. R. Stockwell, *Cell* **2012**, *149*, 1060.
- [13] W. S. Yang, R. SriRamaratnam, M. E. Welsch, K. Shimada, R. Skouda, V. S. Viswanathan, J. H. Cheah, P. A. Clemons, A. F. Shamji, C. B. Clish, L. M. Brown, A. W. Girotti, V. W. Cornish, S. L. Schreiber, B. R. Stockwell, *Cell* **2014**, *156*, 317.
- [14] S. J. Dixon, B. R. Stockwell, *Nat. Chem. Biol.* **2014**, *10*, 9.
- [15] Z. Y. Shen, J. B. Song, B. C. Yung, Z. J. Zhou, A. G. Wu, X. Y. Chen, *Adv. Mater.* **2018**, *30*, 1704007.
- [16] S. Zanganeh, G. Hutter, R. Spitzer, O. Lenkov, M. Mahmoudi, A. Shaw, J. S. Pajarinen, H. Nejadnik, S. Goodman, M. Moseley, L. M. Coussens, H. E. Daldrup-Link, *Nat. Nanotechnol.* **2016**, *11*, 986.
- [17] Z. Y. Shen, T. Liu, J. Lau, Z. Yang, W. P. Fan, Z. J. Zhou, C. R. Shi, C. M. Ke, V. I. Bregadze, S. K. Mandal, Y. J. Liu, Z. H. Li, T. Xue, G. Z. Zhu, J. Munasinghe, G. Liu, A. G. Wu, X. Y. Chen, *ACS Nano* **2018**, *12*, 11355.
- [18] T. Liu, W. L. Liu, M. K. Zhang, W. Y. Yu, F. Gao, C. X. Li, S. B. Wang, J. Feng, X. Z. Zhang, *ACS Nano* **2018**, *12*, 12181.
- [19] Q. H. Sun, Z. X. Zhou, N. S. Qiu, Y. Q. Shen, *Adv. Mater.* **2017**, *29*, 1606628.
- [20] a) A. V. Kroll, R. H. Fang, L. F. Zhang, *Bioconjugate Chem.* **2017**, *28*, 23; b) X. Zhen, P. H. Cheng, K. Y. Pu, *Small* **2019**, *15*, 1804105; c) J. R. Zhou, A. V. Kroll, M. Holay, R. H. Fang, L. F. Zhang, *Adv. Mater.* **2020**, *32*, 1901255.
- [21] L. Rao, L. L. Bu, L. Ma, W. B. Wang, H. Q. Liu, D. Wan, J. F. Liu, A. Li, S. S. Guo, L. Zhang, W. F. Zhang, X. Z. Zhao, Z. J. Sun, *Angew. Chem., Int. Ed.* **2018**, *57*, 986.
- [22] Q. Y. Hu, W. J. Sun, C. G. Qian, C. Wang, H. N. Bomba, Z. Gu, *Adv. Mater.* **2015**, *27*, 7043.
- [23] a) C. Wahl, S. Liptay, G. Adler, R. M. Schmid, *J. Clin. Invest.* **1998**, *101*, 1163; b) C. K. Weber, S. Liptay, T. Wirth, G. Adler, R. M. Schmid, *Gastroenterology* **2000**, *119*, 1209.
- [24] a) J. L. Roh, E. H. Kim, H. J. Jang, J. Y. Park, D. Shin, *Cancer Lett.* **2016**, *381*, 96; b) P. A. Robe, D. H. Martin, M. T. Nguyen-Khac, M. Artesi, M. Deprez, A. Albert, S. Vanbelle, S. Califice, M. Bredel, V. Bours, *BMC Cancer* **2009**, *9*, 372; c) K. Shitara, T. Doi, O. Nagano, C. K. Imamura, T. Ozeki, Y. Ishii, K. Tsuchihashi, S. Takahashi, T. E. Nakajima, S. Hironaka, M. Fukutani, H. Hasegawa, S. Nomura, A. Sato, Y. Einaga, T. Kuwata, H. Saya, A. Ohtsu, *Gastric Cancer* **2017**, *20*, 341; d) M. Dirlik, A. Karahan, H. Canbaz, M. Caghkulekci, A. Polat, L. Tamer, S. Aydin, *Curr. Ther. Res.* **2009**, *70*, 299.
- [25] X. D. Zhang, J. Q. Wang, Z. W. Chen, Q. Y. Hu, C. Wang, J. J. Yan, G. Dotti, P. Huang, Z. Gu, *Nano Lett.* **2018**, *18*, 5716.
- [26] X. L. Wei, M. Ying, D. Dehaini, Y. Y. Su, A. V. Kroll, J. R. Zhou, W. W. Gao, R. H. Fang, S. Chien, L. F. Zhang, *ACS Nano* **2018**, *12*, 109.
- [27] a) L. Rao, L. L. Bu, Q. F. Meng, B. Cai, W. W. Deng, A. Li, K. Y. Li, S. S. Guo, W. F. Zhang, W. Liu, Z. J. Sun, X. Z. Zhao, *Adv. Funct. Mater.* **2017**, *27*, 1604774; b) T. Tan, H. Wang, H. Q. Cao, L. J. Zeng, Y. Q. Wang, Z. W. Wang, J. Wang, J. Li, S. L. Wang, Z. W. Zhang, Y. P. Li, *Adv. Sci.* **2018**, *5*, 1801012.
- [28] a) A. N. Barclay, T. K. Van den Berg, *Annu. Rev. Immunol.* **2014**, *32*, 25; b) L. L. Xu, F. Gao, F. Fan, L. H. Yang, *Biomaterials* **2018**, *159*, 59; c) W. S. Chen, K. Zeng, H. Liu, J. Ouyang, L. Q. Wang, Y. Liu, H. Wang, L. Deng, Y. N. Liu, *Adv. Funct. Mater.* **2017**, *27*, 1605795; d) H. Ye, K. Wang, M. L. Wang, R. Z. Liu, H. Song, N. Li, Q. Lu, W. J. Zhang, Y. Q. Du, W. Q. Yang, L. Zhong, Y. Wang, B. H. Yu,

- H. Wang, Q. M. Kan, H. T. Zhang, Y. J. Wang, Z. G. He, J. Sun, *Biomaterials* **2019**, 206, 1.
- [29] S. K. NaveenKumar, B. N. SharathBabu, M. Hemshekhar, K. Kemparaju, K. S. Girish, G. Mugesh, *ACS Chem. Biol.* **2018**, 13, 1996.
- [30] B. R. Stockwell, J. P. F. Angeli, H. Bayir, A. I. Bush, M. Conrad, S. J. Dixon, S. Fulda, S. K. Hatzios, V. E. Kagan, K. Noel, X. J. Jiang, A. Linkermann, M. E. Murphy, M. Overholtzer, A. Oyagi, G. C. Pagnussat, J. Park, Q. T. Ran, C. S. Rosenfeld, K. Salnikow, D. L. Tang, f. M. Torti, S. V. Torti, S. Toyokuni, K. A. Woerpel, D. D. Zhang, *Cell* **2017**, 171, 273.
- [31] B. Hassannia, B. Wiernicki, I. Ingold, F. Qu, S. V. Herck, Y. Y. Tyurina, H. Bayir, B. A. Abhari, J. P. F. Angeli, S. M. Choi, E. Meul, K. Heyninck, K. Declerck, C. S. Chirumamilla, M. Lahtela-Kakkonen, D. V. Krysko, P. G. Ekert, S. Fulda, M. Conrad, V. E. Kagan, W. V. Berghe, P. Vandenabeele, T. V. Berghe, *J. Clin. Invest.* **2018**, 128, 3341.
- [32] Y. Y. Tyurina, S. M. Poloyac, V. A. Tyurin, A. A. Kapralov, J. F. Jiang, T. S. Anthonymuthu, V. I. Kapralova, A. S. Vikulina, M. Y. Jung, M. W. Epperly, D. Mohammadyani, J. Klein-Seetharaman, T. C. Jackson, P. M. Kochanek, B. R. Pitt, J. S. Greenherger, Y. A. Vladimirov, H. Bayir, V. E. Kagan, *Nat. Chem.* **2014**, 6, 542.
- [33] V. E. Kagan, V. A. Tyurin, J. F. Jiang, Y. Y. Tyurina, V. B. Ritov, A. A. Amoscato, A. N. Osipov, N. A. Belikova, A. A. Kapralov, V. Kini, I. I. Vlasova, M. M. Zou, P. Di, D. A. Svistunenko, I. V. Kurnikov, G. G. Borisenko, *Nat. Chem. Biol.* **2005**, 1, 223.
- [34] S. J. Dixon, B. R. Stockwell, *Annu. Rev. Cancer Biol.* **2019**, 3, 35.
- [35] W. Xie, W. W. Deng, M. H. Zan, L. Rao, G. T. Yu, D. M. Zhu, W. T. Wu, B. Chen, L. W. Ji, L. B. Chen, K. Liu, S. S. Guo, H. M. Huang, W. F. Zhang, X. Z. Zhao, Y. F. Yuan, W. F. Dong, Z. J. Sun, W. Liu, *ACS Nano* **2019**, 13, 2849.
- [36] W. W. Yue, L. Chen, L. D. Yu, B. G. Zhou, H. H. Yin, W. W. Ren, C. Liu, L. H. Guo, Y. F. Zhang, L. P. Sun, K. Zhang, H. X. Xu, Y. Chen, *Nat. Commun.* **2019**, 10, 2025.
- [37] G. De la Rosa, D. Yang, P. Tewary, A. Varadhachary, J. J. Oppenheim, *J. Immunol.* **2008**, 180, 6868.
- [38] R. Yang, J. Xu, L. G. Xu, X. Q. Sun, Q. Chen, Y. H. Zhao, R. Peng, Z. Liu, *ACS Nano* **2018**, 12, 5121.
- [39] W. M. Wang, M. Green, J. E. Choi, P. D. Kennedy, J. K. Johnson, P. Liao, X. T. Lang, I. Kryczek, A. Sell, H. J. Xia, J. J. Zhou, G. P. Li, J. Li, S. Wei, L. Vatan, H. J. Zhang, W. Szeliga, W. Gu, W. P. Zou, *Nature* **2019**, 569, 270.
- [40] H. P. Sun, J. H. Su, Q. S. Meng, Q. Yin, L. L. Chen, W. W. Gu, P. C. Zhang, Z. W. Zhang, H. J. Yu, S. L. Wang, Y. P. Li, *Adv. Mater.* **2016**, 28, 9581.
- [41] J. H. Li, Y. W. Ai, L. H. Wang, P. C. Bu, C. C. Sharkey, Q. H. Wu, B. Wun, S. Roy, X. L. Shen, M. R. King, *Biomaterials* **2016**, 76, 52.
- [42] F. Zhang, F. Li, G. H. Lu, W. D. Nie, L. J. Zhang, Y. L. Lv, W. E. Bao, X. Y. Gao, W. Wei, K. Y. Pu, H. Y. Xie, *ACS Nano* **2019**, 13, 5662.
- [43] R. Aebersold, M. Mann, *Nature* **2003**, 422, 198.
- [44] M. Hayano, W. S. Yang, C. K. Corn, N. C. Pagano, B. R. Stockwell, *Cell Death Differ.* **2016**, 23, 270.
- [45] M. Y. Hu, Y. Wang, L. G. Xu, S. An, Y. Tang, X. F. Zhou, J. J. Li, R. H. Liu, L. Huang, *Nat. Commun.* **2019**, 10, 2993.
- [46] L. C. White, K. L. Wright, N. J. Felix, H. Ruffner, F. I. Reis, R. Pine, P. Y. Ting, *Immunity* **1996**, 5, 365.
- [47] J. Wu, H. D. Zhang, X. M. Shi, X. Xiao, Y. H. Fan, L. J. Minze, J. Wang, R. M. Ghobrial, J. H. Xia, R. Sciammas, X. C. Li, W. H. Chen, *Immunity* **2017**, 47, 1114.
- [48] R. H. Deng, M. Z. Zou, D. W. Zheng, S. Y. Peng, W. L. Liu, X. F. Bai, H. S. Chen, Y. X. Sun, P. H. Zhou, X. Z. Zhang, *ACS Nano* **2019**, 13, 8618.
- [49] D. Chen, J. Xie, R. Fiskesund, W. Dong, X. Liang, J. Lv, X. Jin, J. Liu, S. Mo, T. Zhang, F. Cheng, Y. Zhou, H. Zhang, K. Tang, J. Ma, Y. Liu, B. Huang, *Nat. Commun.* **2018**, 9, 873.
- [50] R. J. Murray, T. A. Wynn, *Nat. Rev. Immunol.* **2011**, 11, 723.
- [51] J. P. F. Angeli, D. V. Krysko, M. Conrad, *Nat. Rev. Cancer* **2019**, 19, 405.